Toxicology 518 (2025) 154262

Contents lists available at ScienceDirect

Toxicology

journal homepage: www.elsevier.com/locate/toxicol

Effects of cigarette smoke extract on surfactant production in ATII-like cells, involvement of oxidative stress and autophagy

Maria Lisa Garavaglia [a,*,1], Francesca Bodega [b,*,1], Chiara Sironi [b], Cristina Porta [b], Isabella Dalle-Donne [a]

[a] Dipartimento di Bioscienze, Università degli Studi di Milano, Milan 20133, Italy
[b] Dipartimento di Fisiopatologia Medico-Chirurgica e dei Trapianti, Università degli Studi di Milano, Milan 20133, Italy

ARTICLE INFO

Keywords:
Surfactant
Cigarette smoke
Alveolar type II cells
SP-B
SP-C
Autophagy

ABSTRACT

Surfactant plays an essential role in pulmonary physiology by reducing surface tension, preventing alveolar collapse, and regulating immune responses in the lung. The composition and function of surfactant can be modified by environmental pollutants. Among these, cigarette smoke is a leading cause of respiratory and cardiovascular diseases. However, the impact of cigarette smoke on surfactant composition and function is still poorly understood. This study evaluated the effects of cigarette smoke extract (CSE) on surfactant production in a differentiated cell model (A549/ATII-like). Specifically, we evaluated the effects of CSE on multilamellar bodies (MLBs) involved in surfactant synthesis and storage, lipid production and secretion, surface tension, and the expression of the surfactant proteins SP-B and SP-C. Since autophagy is involved in MLBs maturation, the expression of SQSTM1/p62 and of the phosphorylated protein pATG-16L1^{S278} was evaluated to assess the effect of CSE exposure on the induction of the early stages of the autophagic process. Our results demonstrated that CSE exposure affects the expression of surfactant components in A549/ATII-like cells, inducing an increase in the surface tension at the air-water interface, possibly via oxidative stress and the alteration of autophagy.

1. Introduction

The alveolar epithelium comprises a simple epithelial sheet constituted by two different cell types: flattened alveolar type I cells (ATI), which account for 95–98 % of the cells and primarily facilitate gas exchange, and type II cells (ATII), which secrete pulmonary surfactant and are involved in alveolar repair and immunomodulation. The epithelium is covered by a tiny aqueous hypophase lined by the pulmonary surfactant, a lipoprotein complex with surface-active properties (Stachowicz-Kuśnierz et al., 2022).

Pulmonary surfactant reduces the surface tension of the fluid that lines the alveoli, thereby decreasing the mechanical work needed to expand the lungs and preventing alveolar collapse. Furthermore, it influences several stages of pulmonary development and is involved in the regulation of immune responses (Bernhard, 2016).

The composition of human pulmonary surfactant differs under different physiological and pathological conditions (Bernhard, 2016; Doyle et al., 1994). Lipids constitute the main component, as they represent approximately 80–90 % (by weight) of surfactant. The majority of lipids are saturated phospholipids, mainly dipalmitoylphosphatidylcholine (DPPC), which is indispensable to reduce the alveolar surface tension. DPPC decreases the cohesion between the water molecules of the lining fluid that covers the alveolar epithelium, thereby preventing alveolar collapse during expiration (Han and Mallampalli, 2015).

Surfactant proteins, which constitute approximately 10–20 % of surfactant, have an important role in regulating its production, maintaining its biophysical properties, and contributing to lung immune defense. The surfactant proteins SP-A and SP-D are members of the collectin family and are involved in the recognition and neutralization of pathogens, as well as in the modulation of inflammatory responses. SP-B and SP-C proteins are members of the saposin family and preserve the stability and the structural organization of the surfactant, avoiding its collapse, also under conditions of high surface tension (Bernhard, 2016; Goerke, 1998). SP-B is also involved in the processing of SP-C (Stahlman et al., 2000) and in the organization of surfactant components into the

* Corresponding authors.
E-mail addresses: maria.garavaglia@unimi.it (M.L. Garavaglia), francesca.bodega@unimi.it (F. Bodega).
[1] Contributed equally

https://doi.org/10.1016/j.tox.2025.154262
Received 9 June 2025; Received in revised form 30 July 2025; Accepted 11 August 2025
Available online 12 August 2025

tightly packed bilayer membranes of the multilamellar bodies (MLBs) (Cañadas et al., 2020; Olmeda et al., 2017). These lysosome-related organelles assemble, store, and secrete the hydrophobic components of surfactant (SP-B, SP-C, and lipids). The transport of the newly synthesized hydrophobic surfactant proteins to MLBs occurs via fusion with multivesicular bodies (MVBs) (Weaver et al., 2002), where the last stages of the SP-B and SP-C processing are completed (Brasch et al., 2004; Stahlman et al., 2000; Weaver et al., 2002) and where the recycling of the extracellular surfactant phospholipids, SP-B, and SP-C takes places after internalization (Weaver et al., 2002). Even though the exact origin of MLBs remains unclear, several studies demonstrated that autophagy appears to be involved in their maturation (Dietl and Frick, 2021; Li et al., 2022; Olmeda et al., 2017).

The lung is an organ highly susceptible to environmental pollutants due to its constant exposure to inhaled air. Cigarette smoke is one of the most harmful air pollutants, and it is a primary cause of respiratory and cardiovascular diseases. Acute and chronic exposure to cigarette smoke induces inflammation and structural damage to the lung tissue, promoting the development of pathological conditions such as chronic bronchitis, chronic obstructive pulmonary disease (COPD), and lung cancer (Adatia et al., 2021; Boo et al., 2023; da Silva et al., 2022; Elisia et al., 2020; Faizan et al., 2025; Fleischmann et al., 2023; Gallucci et al., 2020; Hanrahan et al., 2022; Tyrrell et al., 2023).

Surfactant provides a first line of defense against the effects of cigarette smoke, and its alteration induced by exposure to this pollutant could have remarkable effects, impairing lung function and influencing pathogen clearance through the modulation of the inflammatory cell response (Han and Mallampalli, 2015; Scott, 2004).

Studies investigating the effects of smoking on pulmonary surfactant in humans often report heterogeneous results (Garavaglia et al., 2023).

Understanding how smoke alters both the composition and function of surfactant can offer important insights into the pathophysiology of cigarette smoke-induced respiratory diseases and the progression of chronic conditions such as COPD and lung cancer. Furthermore, this could support the development of therapies useful to restore surfactant function, eventually improving the management and prevention of smoke-related pulmonary diseases.

The aim of our study was to evaluate the effects of cigarette smoke on the lipid and protein composition of surfactant, using an experimental model constituted by A549 cells cultured under conditions that stimulate their differentiation into cells having a phenotype and gene expression profile similar to that of ATII alveolar cells (A549/ATII-like cells) (Cooper et al., 2016). Although this simplified model has disadvantages (Cooper et al., 2016), it provides a reproducible system to analyze the molecular effects of cigarette smoke on surfactant production and avoids the transdifferentiation of ATII cells into the ATI phenotype, observed in primary culture models (Mao et al., 2015).

To this aim, we studied the effect of CSE on both the lipid and the protein components of surfactant produced by A549/ATII-like cells. Specifically, we examined the CSE effects on lipid, SP-B, and SP-C production. Phosphatidylcholine (PC) extracellular levels were analyzed as well. The functional consequences of CSE exposure were analyzed by measuring the surface tension at the air/water interface of the medium where the cells were cultured. Furthermore, since many of the harmful effects of smoking are linked to oxidative stress, immunocytochemical experiments were conducted to determine whether CSE increases the formation of carbonylated proteins, markers of oxidative damage, and whether pretreatment with N-acetylcysteine (NAC), an antioxidant, can reverse the potential toxic effects of CSE exposure.

Finally, since autophagy, which is influenced by oxidative stress as well (Albano et al., 2023; Ning et al., 2023; Ornatowski et al., 2020; Zhao et al., 2022), affects the biogenesis of lamellar bodies (Hariri et al., 2000; Li et al., 2022; Morishita et al., 2020, 2021), we assessed the expression of the sequestosome 1/p62 protein (SQSTM1/p62). This protein serves as a platform for both autophagosome formation and the cellular response to oxidative stress (Chang et al., 2021; Kageyama et al., 2021). p62 possesses two oxidation-sensitive cysteine residues, whose redox sensitivity may represent in vertebrates a mechanism to activate autophagy in response to oxidative stress, hence preserving cellular homeostasis and enhancing cell survival (Carroll et al., 2018; Mehta et al., 2019; van Dam and Dansen, 2020).

Furthermore, we evaluated the expression of Autophagy Related 16-Like 1 (ATG16-L1) protein phosphorylated at serine S278 (pATG-16L1^{S278}), which is a marker of autophagy activation (Runwal et al., 2019; Tian et al., 2020) and regulates several processes, including the inflammatory response (Hamaoui and Subtil, 2022).

2. Materials and methods

2.1. Cell culture

To induce the differentiation of A549 cells to an alveolar type II-like (ATII-like) phenotype, we adopted a long-term culture protocol optimized by Cooper et al. (2016), with minimal modifications. Briefly, 2×10^4 cells/cm^2 A549 cells were seeded into T25 flasks or 24 multiwell and cultured for 23–27 days in Ham's F12 Nutrient Medium (Merk Life Science S.r.l., Italy) supplemented with 2 mM L-Glutamine and 10 % v/v Foetal Bovine Serum (Euroclone). The medium was replaced every 2–4 days. Cells were cultured at 37°C in a humidified incubator with 5 % CO_2. During this extended culture period, cells gradually adopted morphological and molecular features characteristic of ATII-like cells (Cooper et al., 2016). Phase-contrast microscopy was used to monitor monolayer confluence and morphological changes. Cell viability and number were assessed by Crystal Violet assay. Differentiation into ATII-like cells was assessed both morphologically and functionally. The presence of intracellular multilamellar bodies (MLBs), indicative of surfactant storage, was evaluated by TEM microscopy and Oil Red O (ORO) staining (supporting information, figure S2 and S3 a and b). To evaluate the improved functional capacity of the differentiated ATII-like cells to secrete active surfactant components, we measured the ability of the secreted material to reduce surface tension using the drop spreading method (figure S3 c). These combined approaches confirmed that A549 cells cultured under long-term static conditions acquired both structural and functional characteristics of alveolar type II-like cells.

To subculture proliferating cells, cell monolayers were rinsed with phosphate buffered saline (PBS: 137 mM NaCl, 2.7 mM KCl, 10 mM Na2HPO4, and 1.8 mM KH2PO4) and detached from the flask bottom by means of 1x trypsin/EDTA solution (Sigma Aldrich) at 37°C for 9 min. Trypsin was inactivated by the addition of complete growth medium. Cell suspension was centrifuged for 10 min at 1000 rpm and the resulting pellet was resuspended in new medium without trypsin before seeding cells into fresh flasks at a 1:3 ratio.

2.2. Cigarette smoke extract (CSE) preparation and cell treatment

The effect of Marlboro mainstream smoke was analyzed as Marlboro brand alone holds more than twice the world market share of any of its closest competitors (Calafat et al., 2004). The composition of the mainstream smoke of Marlboro cigarettes does not significantly differ from that of reference research cigarettes, nor do their toxicological effects (Patskan et al., 2008).

The method used for CSE preparation was based on protocols by Agraval et al. (Agraval et al., 2022; Colombo et al., 2019), which allowed us to obtain an aqueous solution containing the constituents of cigarette smoke using promptly available equipment. The smoke from a single cigarette (Marlboro, Philip Morris, Inc., Richmond, VA) was bubbled up in 10 ml of complete Ham's F12 medium, and the particulate matter was removed using a 0.45 μm syringe filter. This solution, defined as 100 % CSE, was then diluted to the concentrations of 20, 40, 60 and 80 % in Ham's F12 medium.

An analysis of CSE components has been done by gas chromatography-mass spectrometry (GC-MS) (Kim et al., 2018).

Cells were treated for 3 h with the CSE-containing medium kept at 37°C until the moment of use.

This treatment corresponds nearly to 3, 6, 10, 13, and 16 cigarettes/day for the 20 %, 40 %, 60 %, 80 %, and 100 % CSE solutions, respectively (Su et al., 1998), considering an epithelial lining fluid volume of 20 ml (Fröhlich et al., 2016).

Controls were made by adding fresh Ham's F12 medium to the cultured cells.

After 3 h, cells were rinsed with HBSS (Hanks' Balanced Salt Solution; Sigma Aldrich) at 37°C, followed by a 21 h period of incubation with Ham's F12 medium at 37°C in a humidified 5 % CO2 incubator.

To study the effects of NAC, 2 or 5 mM NAC (Sigma Aldrich) was added 1 h before CSE exposure, followed by a co-treatment for 3 h with 2 or 5 mM NAC and 20 or 40 % CSE respectively. A 50 mM NAC solution in HBSS was freshly prepared immediately before use. The pH of this solution was checked and adjusted to 7.4 using NaOH.

2.3. Cell viability: MTT and crystal violet assay

MTT tests assess cells metabolic activity, evaluating their capability to reduce 3-(4,5-Dimethylthiazol-2-yl)-2,5 diphenyl tetrazolium bromide (MTT) into colored formazan crystals (Ghasemi et al., 2021). A549/ATII-like cells were plated in 24-well plates, allowed to differentiate, and treated with CSE as previously described. After exposure to CSE, the cell culture medium was replaced with MTT (0.5 mg/ml) dissolved in complete growth medium. Cells were then incubated for 90 min at 37°C in a humidified 5 % CO2 incubator. After incubation, the medium was gently removed to avoid the dislodgement of formazan crystals, which were then dissolved by adding 500 μl DMSO (Sigma Aldrich, St. Louis, MO). After 30 min of incubation on an orbital shaker, the absorbance was measured at 590 nm using a plate reader (EnSight multimode microplate reader, Perkin Elmer). Background was measured in wells without cells and was subtracted from the reading.

For the crystal violet assay, A549/ATII-like cells were plated in 24-well plates, allowed to differentiate, and treated with CSE as previously described. Cells were then rinsed twice with PBS (pH 7.4, room temperature) and stained with 0.5 % (w/v) Crystal Violet in 20 % methanol for 10 min at room temperature. After removing the excess of dye by rinsing three times with 1 ml of deionized water, plates were left to dry at room temperature. Crystal Violet was solubilized by adding 1000 μL of methanol per well and incubating for 30 min on an orbital shaker. Absorbance was measured at 570 nm using a microplate reader (EnSight Multimode Microplate Reader, PerkinElmer). Background was measured in wells without cells and was subtracted from the reading.

2.4. Immunofluorescence experiments to assess intracellular levels of carbonylated proteins

To evaluate the intracellular levels of carbonylated proteins, we employed one of the most used methods, based on 2,4-dinitrophenylhydrazine (DNPH) derivatization of carbonyl groups (Colombo et al., 2016). Cells, plated on glass coverslips (#1.5), were fixed and permeabilized by incubation with ice-cold methanol for 5 min. Following three washing steps with TBS (50 mM Tris–Cl, 150 mM NaCl, pH 7.5), cells were exposed to 0.1 % DNPH in 2 N HCl for 1 h. After five washing steps with TBS, the non-specific binding of the antibody to the cells was blocked by exposure to 1 % normal goat serum in TBS for 30 min at RT. Cells were then incubated overnight at 4°C with an anti-DNP antibody (1:500). After three washing steps with TBS, cells were exposed to the secondary antibody (an anti-rabbit TRITC-conjugated, 1:200 in TBS + 0.5 % BSA) for 1 h at RT. Following three additional washing steps, the coverslips were mounted onto glass slides on a drop of aqueous-based mounting medium (90 % glycerol in PBS + 1 % DABCO) and imaged with a Nikon AX R confocal microscope equipped with a Plan APO λD 60x Oil OFN25 DIC N2 objective. The acquired images were analyzed using the Fiji software program, with a region of interest (ROI) selected after thresholding of the images. The threshold was automatically set for all the images using Li's algorithm, which is useful to find an optimal threshold in the presence of the low fluorescence signal observed in the cells under control conditions (Shihan et al., 2021).

2.5. Quantitative Evaluation of Neutral Lipid Levels and Morphologic Analysis of MLBs using Oil Red O

The staining of neutral lipids with Oil Red O (ORO) was performed as reported (Cooper et al., 2016; Mehlem et al., 2013), with some modifications. Namely, a 5 % ORO stock solution in isopropanol was freshly prepared each time. The ORO working solution was obtained by diluting the stock solution at a 4:6 ratio with water, followed by filtration through filter paper and a 0.2 μm syringe filter to remove the insoluble ORO particulate. After eliminating the cell culture medium, cells cultured in 24-well plates were fixed with a 4 % paraformaldehyde solution in PBS, followed by three washing steps with PBS. Subsequently, the ORO working solution was added, and the cells were incubated for 15 min.

For quantitative lipid accumulation analysis, ORO was eluted by isopropanol after repeated washing with double-distilled water to remove the excess of unbound dye. Absorbance was measured spectrophotometrically at 510 nm using a plate reader (EnSight multimode microplate reader, Perkin Elmer).

For morphological analysis of the ORO-stained MLBs, cells cultured on glass coverslips (#1.5) were exposed to Meyer's haematoxylin for 20 min, followed by Scott's tap water to fully develop the blue colour of the nuclei. The coverslips were then mounted on a glass microscope slide for image acquisition using a widefield Nikon microscope equipped with a 40x objective. The images were analyzed with the Fiji analysis program as reported (Deutsch et al., 2014), applying the Huang algorithm for image thresholding after colour deconvolution with the H&E algorithm (Ruifrok and Johnston, 2001).

2.6. Determination of surface tension

The surface tension of the hypophase was estimated using the drop spreading method (Schurch et al., 1978). This method relies on the observation that drops of a variety of nonpolar fluids, placed on top of an air-water interface, change their shape from a sphere to a thin lens when the surface tension increases above a critical value. The surface tension can be determined by the ratio d/d0, where d is the diameter of the drop deposited and d0 is the diameter of the same drop when it has a spherical shape. We used a DMP/O (dimethylphthalate/n-octanol) v/v 4:1 mixture, stained with crystal violet to allow photoimaging of the droplets (Schurch et al., 1978). This fluid is the optimal one to measure surface tension in the range of values expected in our specimens (20–40 mN/m) (Schurch et al., 1978).

On the air-liquid interface of a well where the cells had been seeded and cultured (as described above), a 50 μl droplet of this mixture was placed, and its diameter was determined after taking photographs with a digital camera. Surface tension was determined from the d/d0 ratio, using a calibration curve previously determined (Im Hof et al., 1997).

2.7. Evaluation of phosphatidylcholine release

Phosphatidylcholine (PC) release was evaluated using a commercial kit (phosphatidylcholine colorimetric assay kit; Cayman). In this assay, PC-specific phospholipase is first used to hydrolyze PC to choline and phosphatidic acid. The newly formed choline is then used to generate hydrogen peroxide in a reaction catalyzed by choline oxidase. Finally, with peroxidase as a catalyst, hydrogen peroxide reacts with DAOS (N-ethyl-N-(2-hydroxy-3-sulfopropyl)-3,5-dimethoxyaniline) and 4-aminoantipyrine to generate a blue dye with an optimal absorption at 595 nm.

Briefly, cells were seeded in 96-well plates, grown as described

above, and treated with CSE with or without NAC (as described above). At the end of the treatment, the culture medium was removed and substituted with 100 µl of HBSS, to prevent choline in the medium from interfering with the estimation. After incubation at 37°C in a CO2 incubator for 24 h, the supernatants were removed and allowed to evaporate at 37°C until their volume was reduced to 10 µl. The phosphatidylcholine concentration was then determined using the kit.

2.8. Western blot

Cells were lysed in an SDS lysis buffer with the following composition: 150 mM NaCl, 50 mM Tris-HCl, 1 % (v/v) NP-40, 0.5 % (w/v) sodium deoxycholate, and 2 % SDS, supplemented with protease and phosphatase inhibitor cocktails (Sigma-Aldrich, St. Louis, MO, USA). The lysate was kept on ice for 30 min, and every 10 min was aspirated through the needle of an insulin syringe to reduce its viscosity. The lysate was then centrifuged for 20 min at 12,000 rpm (4°C). The protein concentration of the lysate was determined using a BCA assay (Sigma-Aldrich, St. Louis, MO, USA). Equal amounts of protein (60 µg) were denatured at 37°C for 30 min with 4x Sample Buffer (0.25 M TRIS-HCl pH 6.8, 8 % SDS, 30 % glycerol, 0.02 % bromophenol blue, and 400 mM dithiothreitol (DTT)). DTT was omitted in experiments aimed at examining the SP-B protein as previously described (Subramaniam et al., 1996; Haider et al., 2012). Proteins were separated by tricine sodium dodecyl sulphate–polyacrylamide gel electrophoresis (SDS-PAGE). After loading the samples into the wells of the stacking gel, the electrophoresis was run at 90 V for 20 min, followed by 140 V for 90 min. The separated proteins were then transferred onto PVDF (polyvinylidene fluoride) membranes (Bio-Rad, Italy).

The membranes were blocked for 1 h at RT in Tris-buffered saline with 0.1 % (v/v) Tween 20 (TBST) containing 5 % skim milk (Biorad, Italy) or, just for the pATG16-L1^{s278} Western blot, 5 % BSA (Sigma, Italy). Immunoblotting was then performed by incubating the membranes overnight at 4°C with the appropriate primary antibodies diluted in 5 % skim milk in TBST. Following washing with TBST, the membranes were incubated with horseradish peroxidase (HRP)-conjugated secondary antibodies for 1 h at RT. After three washing steps, protein detection was carried out using an enhanced chemiluminescence (ECL) kit (Thermo Fisher Scientific) according to the manufacturer's instructions. The protein bands were visualized using the ChemiDoc Touch System (Bio-Rad Laboratories, Italy) and quantified via densitometric analysis with Fiji software (ImageJ, NIH, USA, Version 1.54, 5 December 2024). Data were normalized to GAPDH, used as the loading control.

The SP-B and SP-C antibody specificity was tested on HeLa cell lysates (Fig. S5 and S6).

In order to reduce the variability due to analytical variations in Western blotting, we normalized Western blot replicates by the "sum of the replicates" method, as reported (Degasperi et al., 2014).

The concentration and type of primary antibodies, along with the corresponding secondary antibodies used in the experiments, are summarized in Table 1.

Table 1
Concentrations and types of primary and secondary antibodies used in Western blot experiments.

Primary Antibody	Concentration	Secondary Antibody	Concentration
Anti-SP-B rabbit monoclonal SAB5600258 (Sigma-Aldrich)	1:500	Goat anti-Rabbit IgG (H+L) Cross-Adsorbed Secondary Antibody, HRP cod. G21234 (Invitrogen)	1:10000
Anti-SFTPC rabbit polyclonal MBS9408251 (MyBioSource)	1:500	Goat anti-Rabbit IgG (H+L) Cross-Adsorbed Secondary Antibody, HRP cod. G21234 (Invitrogen)	1:10000
Anti-GAPDH mouse monoclonal G8795 (Sigma-Aldrich)	1:20000	Goat Anti-Mouse IgG (H + L)-HRP Conjugate #1706516 (Cell Signaling Technology)	1:10000
Anti-ATG16L1 (phospho S278) rabbit monoclonal ab195242 (Abcam)	1:10000	Goat anti-Rabbit IgG (H+L) Cross-Adsorbed Secondary Antibody, HRP cod. G21234 (Invitrogen)	1:10000
Anti- SQSTM1/p62 mouse monoclonal ab56416 (Abcam)	1:10000	Goat Anti-Mouse IgG (H + L)-HRP Conjugate #1706516 (Cell Signaling Technology)	1:10000

2.9. Immunofluorescence (IF) analysis

For immunofluorescence (IF) analysis of SP-C and SP-B proteins, cells cultured on coverslips (#1.5) were rinsed with PBS and fixed with 4 % paraformaldehyde in PBS for 15 min. After three washes with PBS lasting 5 min each, cells were permeabilized using 0.1 % saponin in PBS for 10 min. Non-specific binding sites were blocked with 5 % normal goat serum (NGS) and 0.1 % saponin in PBS for 60 min. Cells were then incubated overnight at 4°C with primary antibodies: 1:500 anti-SP-B rabbit monoclonal (SAB5600258, Sigma-Aldrich) or 1:250 anti-SFTPC rabbit polyclonal (MBS9408251, MyBioSource) in blocking buffer (0.1 % saponin and 1 % NGS in PBS). After three other washing steps with PBS, cells were incubated with TRITC-conjugated secondary antibody (Rhodamine (TRITC) AffiniPure® Goat Anti-Rabbit IgG (H+L), AB_2337926, Jackson ImmunoResearch) for 1 h at RT in the dark. Finally, nuclei were counterstained with 1 µg/ml 4,6-diamidino-2-phenylindole (DAPI, Sigma-Aldrich) in PBS for 10 min.

For ATG-16 and p62 co-immunofluorescence, cells were fixed with 4 % paraformaldehyde in PBS, permeabilized and blocked with 0.1 % saponin and 2 % NGS in PBS for 10 min, and then incubated with the primary antibody (1:150 Anti-ATG16L1 [phospho S278] rabbit monoclonal, ab195242, Abcam) in blocking buffer overnight at 4°C. After three washing steps with PBS, cells were incubated with the secondary anti-rabbit FITC antibody (Fluorescein (FITC) AffiniPure™ Goat Anti-Rabbit IgG, AB_2337972, Jackson ImmunoResearch), diluted 1:250 in 200 µl PBS with 1 % NGS, for 1 h at RT. Following three additional PBS washes, permeabilization and blocking were repeated with 0.1 % saponin and 2 % NGS in PBS for 10 min. Cells were then incubated with the primary antibody for p62 (1:150 Anti-SQSTM1/p62 mouse monoclonal, ab56416, Abcam) in blocking buffer for 24 h at 4°C. On the following day, after removal of the solution and three PBS washes, the cells were incubated with the secondary anti-mouse Cy5 antibody (Cy5® goat anti-mouse IgG (H+L), Catalog Number 16855, AAT Bioquest), diluted 1:250 in PBS with 1 % NGS, for 1 h at RT. After five washes with PBS, cells were exposed to DAPI (1 µg/ml) for 10 min, followed by three final washes with PBS.

The coverslips were mounted onto glass slides with a drop of aqueous-based mounting medium (90 % glycerol in PBS + 1 % DABCO) and images were captured with a Nikon AX R confocal microscope equipped with a Plan APO λD 60x Oil OFN25 DIC N2 objective.

Image analysis was performed using the Fiji analysis program. The regions of interest (ROIs) were selected after thresholding of images using the Huang algorithm, which is appropriate for images where the pixel intensity distribution does not follow a normal distribution.

2.10. Statistical analysis

The data are expressed as mean ± standard error of the mean (SEM). Statistical comparison was performed with the programs OriginPro 2021b (64-bit) SR2 or Excel 2019 (Microsoft). The normality of the data distribution was assessed by the Kolmogorov-Smirnov test. For the data that did not show a normal distribution, the statistical test was performed by non-parametric tests (one-way ANOVA Kruskal–Wallis test,

followed by multiple comparison with Dunn's test for the comparison of more than two groups). If the data followed a normal distribution, the statistical test was performed by one- or two-way ANOVA, followed by multiple comparisons with Bonferroni's test for the comparison of more than two groups. For all studies, values were considered significantly different at $p < 0.05$ or $p < 0.01$, as indicated.

3. Results

3.1. A549/ATII-like cell viability is affected by CSE

CSE contains numerous highly toxic compounds (Centers for Disease Control and Prevention, 2010). To assess the impact of different concentrations (20 %, 40 %, 60 %, 100 %) of CSE on A549/ATII-like cell viability, experiments were conducted using the MTT assay. The viability of cells exposed to 100 % and 80 % CSE was significantly reduced compared to the control group. In contrast, no significant changes in viability were observed in cells exposed to 20 %, 40 %, and 60 % CSE (Fig. 1), demonstrating that these conditions do not affect cell metabolic activity (Ghasemi et al., 2021).

Additional experiments were conducted using the crystal violet (CV) assay to indirectly evaluate the number of adherent cells following exposure to the same concentration of CSE used in the MTT experiment (Feoktistova et al., 2016). Cell number significantly decreased, compared to control conditions, when cells were exposed to 100 %, 80 %, and 60 % CSE (Fig. 1B).

The partial discrepancy observed after 60 % CSE exposure between the MTT and Crystal Violet assays likely reflects the different biological aspects evaluated by these methods—metabolic activity versus cell number—rather than a methodological artefact, as previously reported (Kardorff et al., 2023). This supports the use of complementary viability assays to gain a more complete picture of cellular conditions following toxic exposures.

On the whole, these results showed that 20 % and 40 % CSE exposure did not significantly affect the viability in A549/ATII-like cells, making these the conditions appropriate for further experiments designed to evaluate the molecular effects of CSE exposure on surfactant production and regulation.

3.2. CSE-induced oxidative stress in A549/ATII-like cells: immunocytochemical analysis of intracellular protein carbonylation

Cigarette smoke causes oxidative stress in several cell types both in vivo and in vitro (Cipollina et al., 2022; van der Vaart, 2004). Since carbonylation is a well-established hallmark of cellular oxidative damage (Dalle-Donne et al., 2017, 2003a, 2003b), we performed immunodetection of intracellular protein carbonylation to assess whether the oxidative stress induced by 20 % and 40 % CSE exposure is sufficient to elicit downstream molecular alterations in A549/ATII-like cells, even if not affecting cell viability. Additionally, in some experiments, cells were pretreated with the antioxidant N-acetylcysteine (NAC) (Kosmider et al., 2011; Wang et al., 2017) to set out the experimental conditions that could mitigate the CSE-induced oxidative damage. Based on the available literature (Hoshino et al., 2001; Hur et al., 2022; Khanna et al., 2012), we established a treatment protocol including a one-hour pre--treatment with NAC, followed by a co-treatment with CSE and NAC (2 mM NAC with 20 % CSE and 5 mM NAC with 40 % CSE). Exposure to NAC or NAC and CSE at the concentration used did not affect cell viability (Fig. S1).

After CSE exposure (Fig. 2), A549/ATII-like cells showed a significant increase in intracellular protein carbonylation, confirming that oxidative stress is present even at concentrations that do not impact cell viability, as previously observed in other cell types (Colombo et al., 2019; Gornati et al., 2013). This effect was CSE concentration-dependent, as 40 % CSE induced significantly higher carbonylation than 20 % CSE. Notably, NAC treatment significantly reduced protein carbonylation, confirming its protective role against CSE-induced oxidative stress (Caito et al., 2010; Colombo et al., 2019; Higashi et al., 2019).

A one-hour pre-treatment with 2 mM NAC, maintained throughout the 20 % CSE exposure, significantly reduced the intracellular protein carbonylation to levels not significantly different from those in control cells. However, in the presence of 40 % CSE, even with a higher concentration of NAC (5 mM), intracellular protein carbonyl levels were significantly higher than in control cells, although significantly reduced compared to those observed in the absence of the antioxidant. Higher concentrations of NAC were not tested, as previous studies have reported a cytotoxic effect along with an inhibition on A549 cell growth at elevated NAC doses (Liao et al., 2021; Wong et al., 2023).

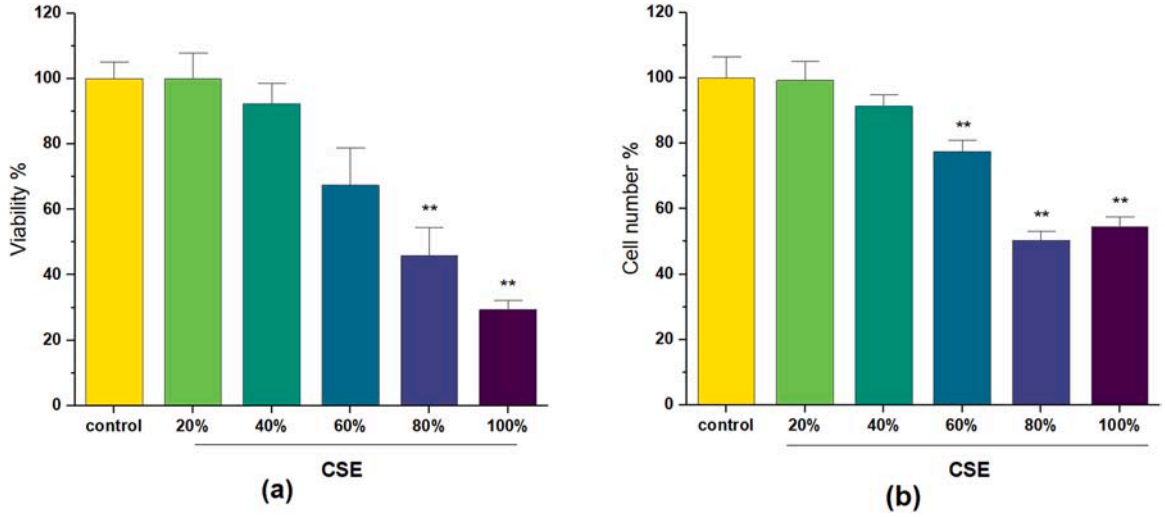

Fig. 1. Effect of CSE on A549/ATII-like cell viability. A) assessment of changes in cell viability following exposure to different concentrations of CSE. B) evaluation of the alteration in cell number after exposure to different concentrations of CSE. Data are expressed as a percentage relative to control and reported as mean ± SEM. ** = $p < 0.01$, respectively, compared to control, with the one-way ANOVA test (n = 9 and 12 for MTT and CV assays, respectively).

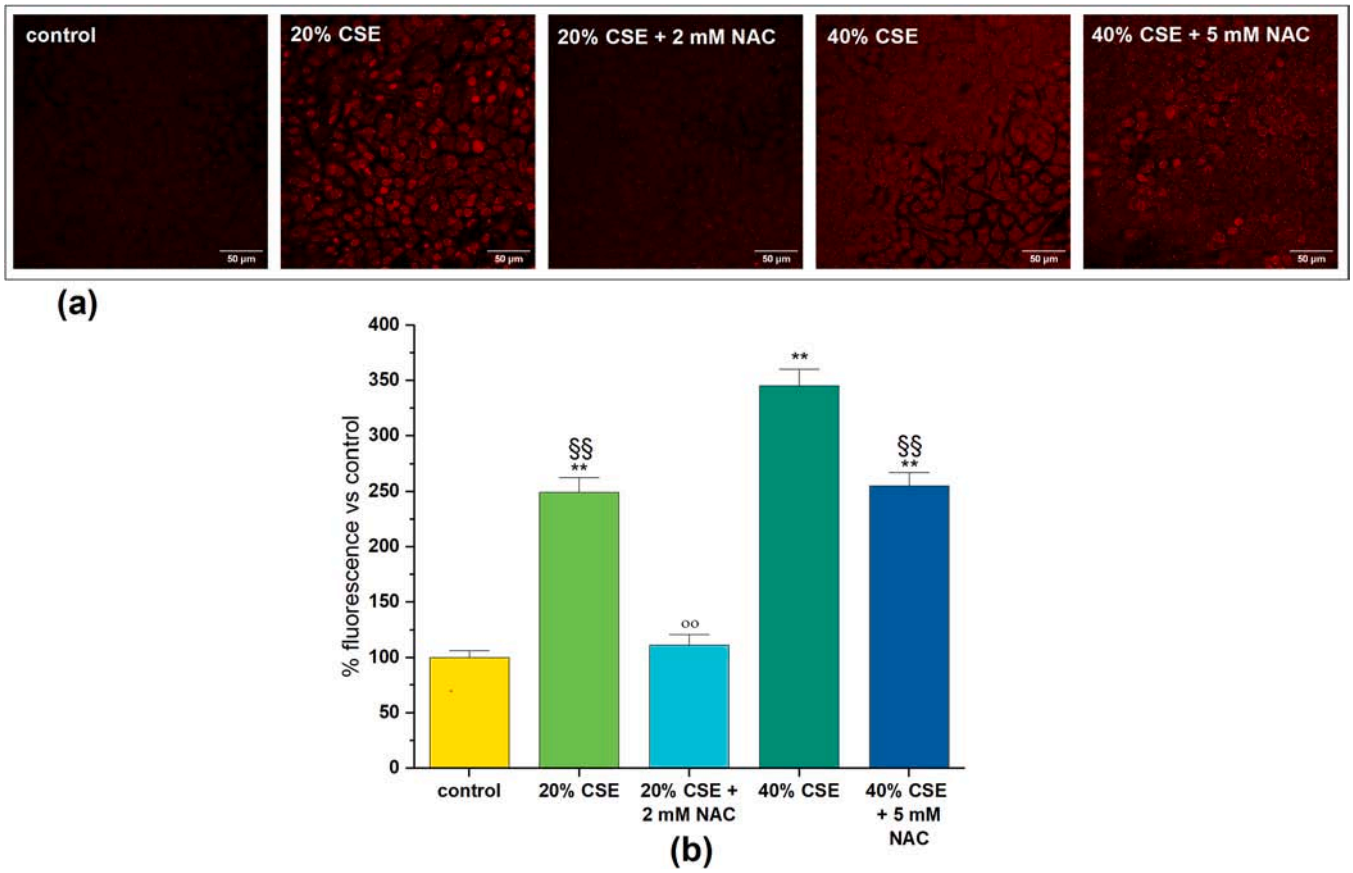

Fig. 2. CSE affects intracellular protein carbonylation in A549/ATII-like cells. A) Representative immunofluorescence images showing global protein carbonylation after 3 h of CSE or CSE + NAC exposure. As a negative control, no immunostaining was observed in parallel experiments in which the primary antibody to 2,4-dinitrophenylhydrazine (DNP) was omitted (not shown). Scale bar = 50 µm. B) Semi-quantitative analysis of the immunofluorescence images performed using the Fiji analysis program. Fluorescence is measured as percentages relative to control. The data are presented as mean ± SEM. ** = $p < 0.01$ compared to control, °° = $p < 0.01$ compared to 20 % CSE, §§ = $p < 0.01$ compared to 40 % CSE, with the one-way ANOVA test (n = 18, 18, 13, 18, 13 images from three independent experiments for control, 20 % CSE, 40 % CSE, 20 % CSE + 2 mM NAC, 40 % CSE + 5 mM NAC, respectively).

3.3. Neutral lipid content and multilamellar body morphology in A549-ATII-like cells are influenced by CSE exposure

ATII cells are characterized by the presence of MLBs, which store surfactant lipids and proteins, and MVBs, which deliver SP-B and SP-C to lamellar bodies. Using transmission electron microscopy (Fig. S2), we confirmed the presence of both MLBs and MVBs in A549/ATII-like cells at 21–25 days of differentiation. Notably, we observed no other types of lipid droplets, as previously reported (Cooper et al., 2016).

Based on this observation, neutral lipid accumulation in MLBs was assessed using Oil Red O (ORO) staining, which enables a more straightforward quantitative and morphological analysis. Monolayers of A549/ATII-like cells were stained with ORO alone for spectrophotometric quantification of the intracellular neutral lipid content, while combined ORO and haematoxylin staining allowed us to morphologically evaluate MLBs following CSE exposure.

As an initial assessment, the time-dependent differentiation of A549/ATII-like cells was analyzed with these methods. Our results showed that there was a greater accumulation of lipid in MLBs when cells were cultured in Ham's F12 compared to the standard D-MEM (Fig. S3), confirming that these culture conditions promote cell differentiation, as reported (Cooper et al., 2016).

The intracellular neutral lipid content was reduced after exposure to different concentrations of CSE, with a significant effect already after 20 % CSE exposure (Fig. 3).

These data are not due to variations in cell number, as confirmed by the Crystal Violet assay (Fig. 1b).

The decrease in intracellular lipid content was confirmed through the analysis of immunocytochemical images of control and CSE-exposed A549/ATII-like cells. Compared to the control, 40 % CSE exposure significantly reduced both the total area occupied by MLBs and the number of MLBs, but not their mean size. Assuming, as an approximation, a perfectly circular shape of the MLBs, the estimated mean diameters were 1.09 ± 0.02 µm (n = 24 images), 1.07 ± 0.02 µm (n = 20 images), and 1.05 ± 0.02 µm (n = 16 images) in control conditions or after 20 % and 40 % CSE exposure, respectively. These measurements are in agreement with previously reported values (Schmitz and Müller, 1991).

These results unveil that the CSE-induced reduction in neutral lipid content is attributable to a decrease in the number of MLBs, rather than a reduction in their size.

To determine whether the effect of CSE on neutral lipid content and MLB morphology could be influenced by oxidative stress, identical experiments were performed in the presence of NAC (Fig. 4).

The intracellular lipid levels and the number of MLBs in 20 % and 40 % CSE-exposed cells returned to values comparable to those observed in control conditions with NAC treatment.

3.4. CSE exposure increases surface tension at the air-liquid interface of A549/ATII-like cell cultures

To assess whether CSE exposure modifies surfactant function, the surface tension at the air-liquid interface of wells where the cells had been seeded and cultured was measured using the drop spreading

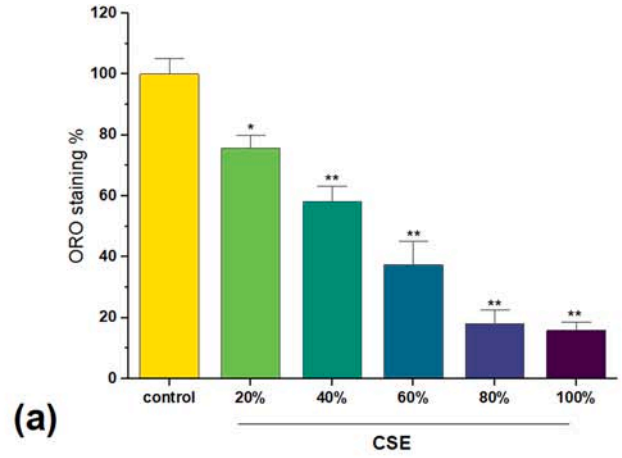

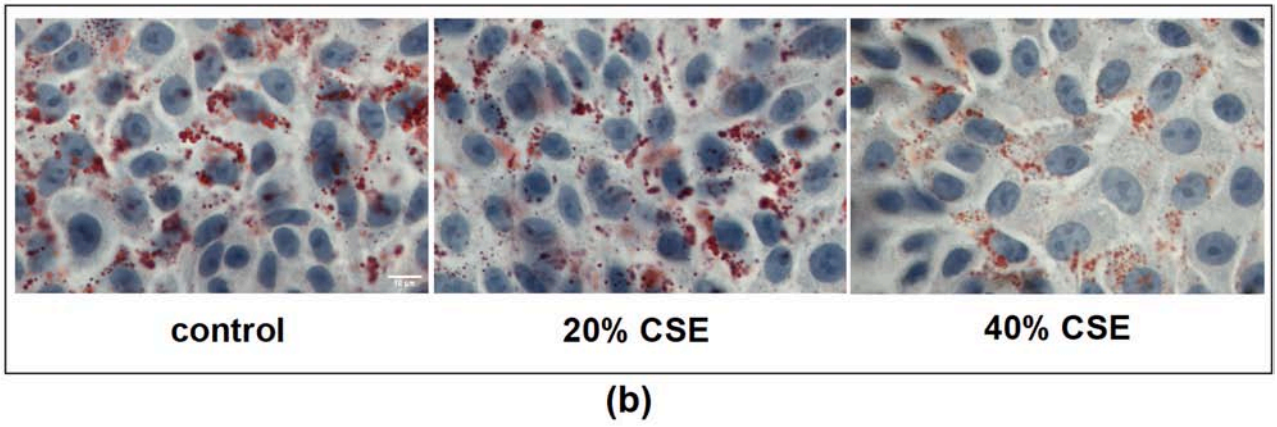

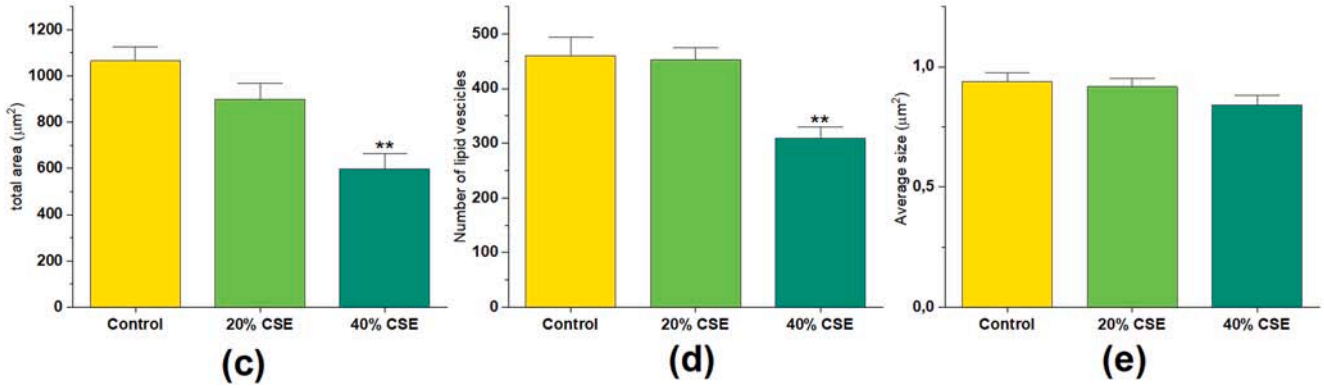

Fig. 3. Effect of CSE on intracellular neutral lipid content and MLB morphology in A549/ATII-like cells. A) Quantification of intracellular lipid content, reported as a percentage relative to control after exposure to different concentrations of CSE (n = 12 per condition tested). B) Representative immunocytochemical images of A549/TII-like cells stained with ORO (for MLBs visualization) and haematoxylin (for nuclei) in control conditions and after 20 % or 40 % CSE exposure. Scale bar = 10 μm. **C)** Quantification of the total area (in μm2) covered by all MLBs in the images acquired in control conditions or after 20 % or 40 % CSE exposure (n = 24, 20, 20 images acquired from 6, 5 and 5 different samples, respectively). D) and E) Mean number and area (μm^2) of MLBs in control and in 20 % or 40 % CSE-exposed cells (n = 24, 20, 20 images acquired in 6, 5 and 5 different samples, respectively). Data are reported as mean ± SEM. *, ** = $p < 0.05$, 0.01 respectively (compared to control) with the one-way ANOVA test. Image analysis was performed by Fiji software.

method, that allowed us to evaluate surface tension in a controlled in vitro setting by measuring the size of a dimethylphthalate/n-octanol mixture drop placed on the air-liquid interface (Schurch et al., 1978). This approach has been used in both tissue and cultured cell studies (Blank et al., 2006; Im Hof et al., 1997; Nalayanda et al., 2010; Öhlinger et al., 2019; Schurch et al., 1978). Cells cultured for 24 days in Ham's F12 had a surface tension significantly lower than the same cells cultured for 24 days in D-MEM. Moreover, in cells cultured in Ham's F12, surface tension decreased with time of culture (Figure S3). As shown in Fig. 5, treatment with both 20 % and 40 % CSE induced significant increases in surface tension. The maximum effect was achieved already following 20 % CSE exposure, and NAC did not exert any protective effect. These results cannot be attributable to a reduction in the number of cells in culture, as evidenced by experiments conducted using the CV technique, which demonstrated that neither 20 % CSE nor 40 % CSE exposure affected cell number (Fig. 1b). Notably, the surface tension value measured in our control samples (32.9 mN/m) was consistent with those measured in previous studies on A549 cells, cultured at an

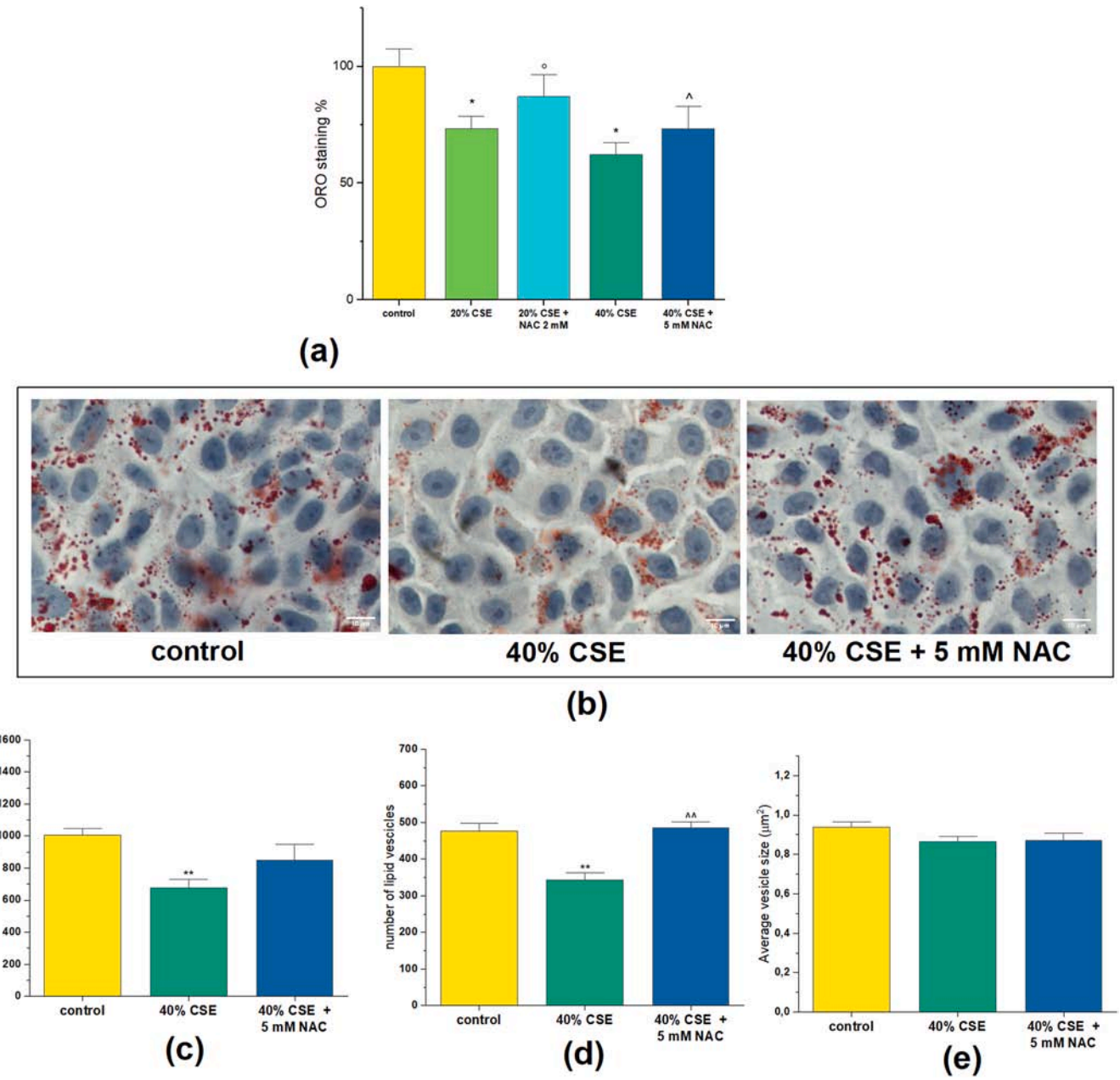

Fig. 4. Modulation by NAC of the CSE effect on intracellular neutral lipid content and MLB morphology in A549/ATII-like cells. A) Quantification of intracellular lipid content reported as a percentage relative to control, following exposure to 20 % or 40 % CSE, with or without NAC (n = 38, 43, 31, 22, 10 for each condition). B) Representative images of A549/ATII-like cells stained with ORO (for MLBs) and haematoxylin (for nuclei) under control conditions, after 40 % CSE exposure, and after 40 % CSE + 5 mM NAC exposure. Scale bar = 10 μm. C) Quantification of the total area (in μm^2) covered by all MLBs in the images acquired under control conditions or after 40 % CSE or 40 % CSE + 5 mM NAC exposure (n = 24, 20, 20 images acquired in 6, 5 and 5 different samples, respectively). D) and E) Mean MLBs number and area (μm2) in control condition or after 40 % CSE or 40 % CSE + 5 mM NAC exposure (n = 24, 20, 20 images acquired in 6, 5 and 5 different samples, respectively). Data are reported as mean ± SEM. *, ** = $p < 0.05$, 0.01 respectively compared to control; ° = $p < 0.05$ compared to 20 % CSE; ^, ^^ = $p < 0.05$, 0.01 respectively compared to 40 % CSE, with the one-way ANOVA test. Analysis of the images was performed by Fiji software.

air-liquid interface (ALI) to promote an ATII phenotype, where surface tension was ~30 mN/m, compared to a value of ~45 mN/m in non-differentiated cells (Blank et al., 2006; Nalayanda et al., 2010; Öhlinger et al., 2019), supporting the use of A549/ATII-like cells as a relevant model for surfactant function studies.

These results suggest that CSE exposure impairs surfactant function by increasing surface tension, which could cause alveolar instability and respiratory dysfunction.

3.5. CSE exposure does not affect extracellular PC levels

The low surface tension of the alveolar lining fluid depends mainly on the presence of PC in the surfactant. Consequently, we investigated if the effects of CSE on the surface tension were due to a reduction in extracellular levels of PC.

As shown in Fig. 6, 20 % or 40 % CSE exposure, with or without NAC, did not induce any significant variation in the levels of extracellular PC.

These results unveil that the increase in surface tension induced by CSE is not generated by a reduction in the levels of PC. Instead, other

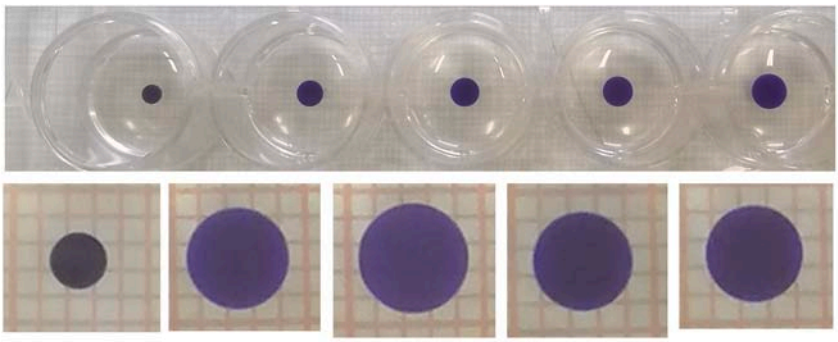

(a)

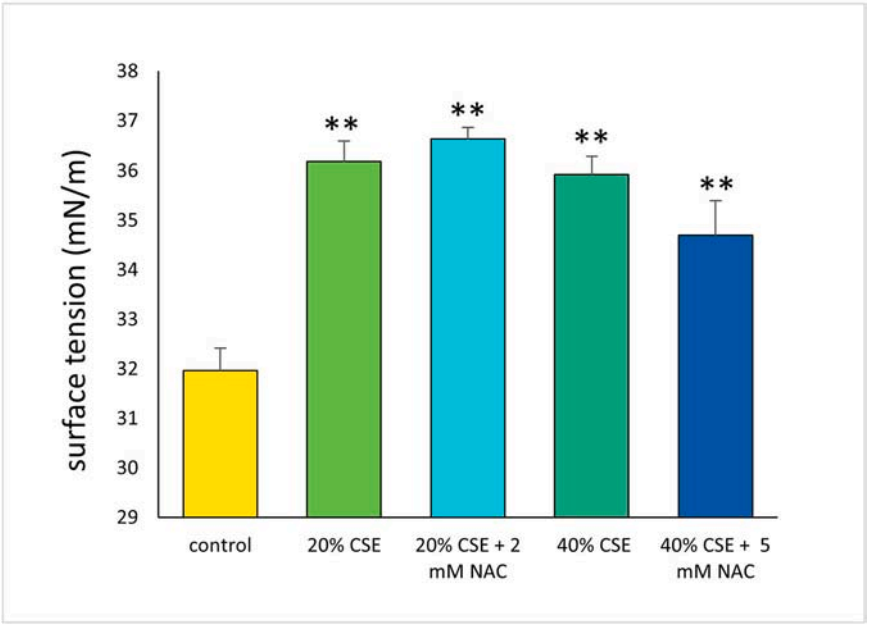

(b)

Fig. 5. Effect of CSE on surface tension at the air-liquid interface of wells where the cells had been seeded and cultured, measured using the drop spreading method. A) Representative images of dyed dimethylphthalate/octanol droplets on A549/ATII-like cells in control conditions and after 20 % or 40 % CSE exposure, with or without NAC. B) Surface tension measurements calculated from the droplet diameter in the control condition and after 20 % or 40 % CSE exposure, with or without NAC. Data are reported as mean ± SEM. ** = $p < 0.01$ (compared to control) with the one-way ANOVA test (n = 38, 23, 23, 15, 16).

factors, such as alterations in surfactant protein composition or in surfactant metabolism, can produce the observed impairment in surfactant function. Further investigations have been carried out to elucidate this observation.

3.6. CSE modulates intracellular expression and localization of surfactant proteins SP-B and SP-C

To investigate the effect of CSE on the intracellular levels and localization of SP-B and SP-C, two distinctive proteins of pulmonary surfactant that modulate its rheological characteristics and surface-active properties (Liekkinen et al., 2023; Schürch et al., 2010), we conducted Western blot and immunofluorescence experiments.

3.6.1. SP-B

Western blot experiments were performed to evaluate the effect of CSE on SP-B protein expression levels, using an antibody targeting an amino acid sequence within the mature SP-B protein. This approach allowed us to detect both the mature form and its intracellular protein intermediates (Banfi and Agostoni, 2016; Korimilli et al., 2000) (Fig. 7).

A significant increase in mature SP-B levels was observed after exposure to 40 % CSE, which was not reversible in the presence of NAC.

The ratio between mature SP-B and pre-SP-B (Fig. 7f) increases significantly during 40 % CSE exposure, suggesting intracellular accumulation of mature SP-B, and this effect was not prevented by NAC.

Immunofluorescence experiments were conducted to confirm these results and to evaluate changes in the intracellular distribution of the protein. An increase in protein expression was observed in the presence of 40 % CSE, not reversible after 5 mM NAC exposure (Fig. 8).

The integrated density significantly increased in 20 % and 40 % CSE-treated cells compared to the control. This increase was due to a larger cellular area expressing the fluorescent protein and, for the 40 % CSE-exposed cells, to a higher mean fluorescence intensity.

In control conditions the fluorescence intensity distribution exhibited a high positive skewness and kurtosis, suggesting a non-uniform distribution of fluorescence (NIST,). Skewness is an index of the

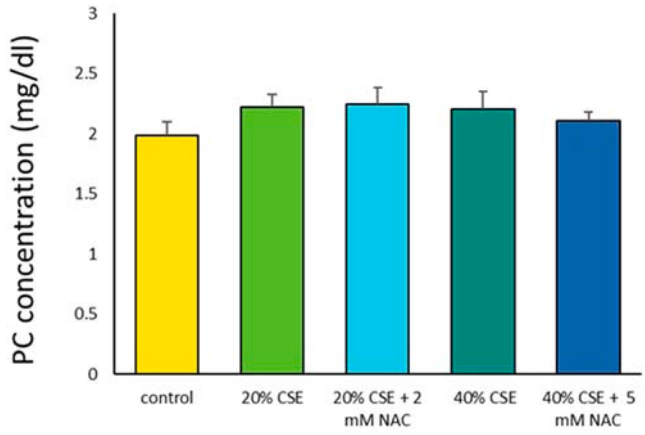

Fig. 6. Influence of CSE (with or without NAC) on the extracellular PC concentration. Data are reported as mean ± SEM, analyzed with the one-way ANOVA test (n = 19, 19, 12, 12, 12).

asymmetry of the intensity distribution. A positive skewness indicates that most of the fluorescence intensity values form a tail extending toward higher intensities. Kurtosis is an index showing whether the data are heavy- or light-tailed if compared to a normal distribution and, in this case, a high kurtosis is in agreement with the presence of a distribution with heavy tails or outliers, corresponding to areas of high fluorescence intensity, such as vesicles where immunofluorescence signals are clustered. After treatment with 40 % CSE, both skewness and kurtosis significantly decreased compared to the control, suggesting a more uniform distribution of fluorescence. Notably, the observation of the higher magnification images (Fig. 7a) revealed that, in 40 % CSE-exposed cells, fluorescence was more prominent in the cytoplasm, particularly in perinuclear tubular structures and small vesicles. 5 mM NAC did not reverse the CSE-induced effect: the values of integrated density, skewness and kurtosis remained significantly different from those observed in control conditions.

It is worth noting that, after exposure of the cells to 20 % CSE, a trend toward increased expression of both pre-SP-B and the mature form was observed by Western blot analysis, which was not statistically significant. However, this increase reached statistical significance when assessed by immunofluorescence. This discrepancy may be due to the higher sensitivity of immunofluorescence in detecting protein local expression variation caused by spatial redistribution in subcellular compartments. While Western blot measures average protein levels in the whole-cell lysate, potentially masking moderate or localized changes, immunofluorescence can highlight differences of protein distribution and abundance that may be functionally relevant. Importantly, the measurement of surface tension revealed a significant alteration already after 20 % CSE cell exposure, supporting the functional significance of the immunofluorescence findings. The observed SP-B redistribution within the cytoplasm and vesicular compartments correlates with surfactant dysfunction. This suggest that changes in SP-B localization or compartmentalization may lead by itself to an alteration of surfactant function.

3.6.2. SP-C

The effect of CSE exposure on SP-C expression was assessed using Western blot, employing an antibody for the C-terminal region of the SP-C precursor protein (Pre-SP-C). The mature isoform of SP-C is, in fact, a highly lipophilic, low-molecular-weight protein (3.7 kDa), making its analysis by Western blotting complex (Fig. 9).

Exposure to 40 % CSE resulted in a significant reduction in ProSP-C expression, whereas 20 % CSE had no effect. However, protein expression returned to levels not significantly different from control in cells exposed to 40 % CSE and 5 mM NAC.

Immunofluorescence experiments were performed to assess the Western blot results and to evaluate changes in the localization and distribution of SP-C protein within the cells following CSE exposure (Fig. 10).

40 % CSE exposure induced a significant decrease in integrated density, mean intensity, and area. NAC appeared to exert a partial protective effect, as the addition of NAC (5 mM) to 40 % CSE resulted in an increase in the fluorescent signal area, which was not significantly different from the control. Conversely, 20 % CSE exposure did not significantly affect protein expression: the significant decrease in mean fluorescence intensity in the cells was compensated by an increase in the fluorescent signal area, keeping the integrated density unchanged.

In contrast to what was observed for SP-B, skewness and kurtosis did not statistically change, indicating that the distribution patterns of pro-SP-C did not undergo major alterations following the treatments, despite some trends suggesting that NAC might have a modulatory effect.

These results indicate that CSE exposure differentially affects SP-B and SP-C expression in A549/ATII-like cells. While SP-B accumulates intracellularly, likely due to processing alterations, SP-C levels decrease, indicating possible disruptions in surfactant homeostasis.

3.7. CSE Modulation of autophagy induction: evidence from p62 and pATG16-L1^{S278} protein expression and localization

Although the intracellular mechanisms involved in the formation and maturation of MLBs have not been fully elucidated, it is known that autophagy plays a part in MLBs maturation (Li et al., 2022). Therefore, we investigated whether CSE could influence the autophagic process in A549/ATII-like cells. In particular, we analyzed the effect of CSE exposure on sequestosome 1 (SQSTM1/p62), a scaffold protein that serves as a platform for autophagosome formation during oxidative stress response ((Kageyama et al., 2021), and on the Autophagy Related 16-Like 1 protein (ATG16-L1) phosphorylated at serine 278 (pATG16-L1^{S278}). pATG16-L1^{S278} is a marker of the autophagic process more reliable than microtubule-associated protein light chain 3 (LC3B) (Runwal et al., 2019; Tian et al., 2020). Furthermore, LC3B has been shown to colocalize with the limiting membrane of the MLBs (Li et al., 2022). ATG16-L1, forming a complex with other proteins, is known to interact with LC3B, thereby remodelling the membrane to form cup-like structures (Mohan et al., 2024).

To investigate the effect of CSE on p62 and pATG16-L1^{S278} expression, we performed Western blot analysis following treatment with CSE or CSE + NAC (Fig. 11).

Following 40 % CSE exposure, a significant increase in p62 and a decrease in pATG16-L1^{S278} levels were observed, in agreement with a possible alteration of autophagy. The exposure to NAC modulated this effect, restoring protein levels to control values.

Consistent results were obtained from immunofluorescence experiments, where the expression of both proteins in cells was assessed (Fig. 12). In this case as well, the effect was reversible upon treatment with NAC.

However, the colocalization area where both signals for p62 and pATG16-L1^{S278} were present was significantly reduced following 20 % and 40 % CSE exposure. This indicates a disruption in the formation of p62 bodies, which serve as precursors for autophagy activation. Notably, this effect was not reversed in the presence of NAC, thus indicating that CSE-induced alterations in p62 and pATG16-L1^{S278} interactions continue even during treatment with the antioxidant.

These results indicate that CSE exposure disrupts autophagy-related processes in A549/ATII-like cells. This could impair MLBs maturation.

4. Discussion

Cigarette smoke represents a major public health threat, containing thousands of toxic chemicals that reach the upper airways and alveoli, with many effects, which include surfactant homeostasis and function

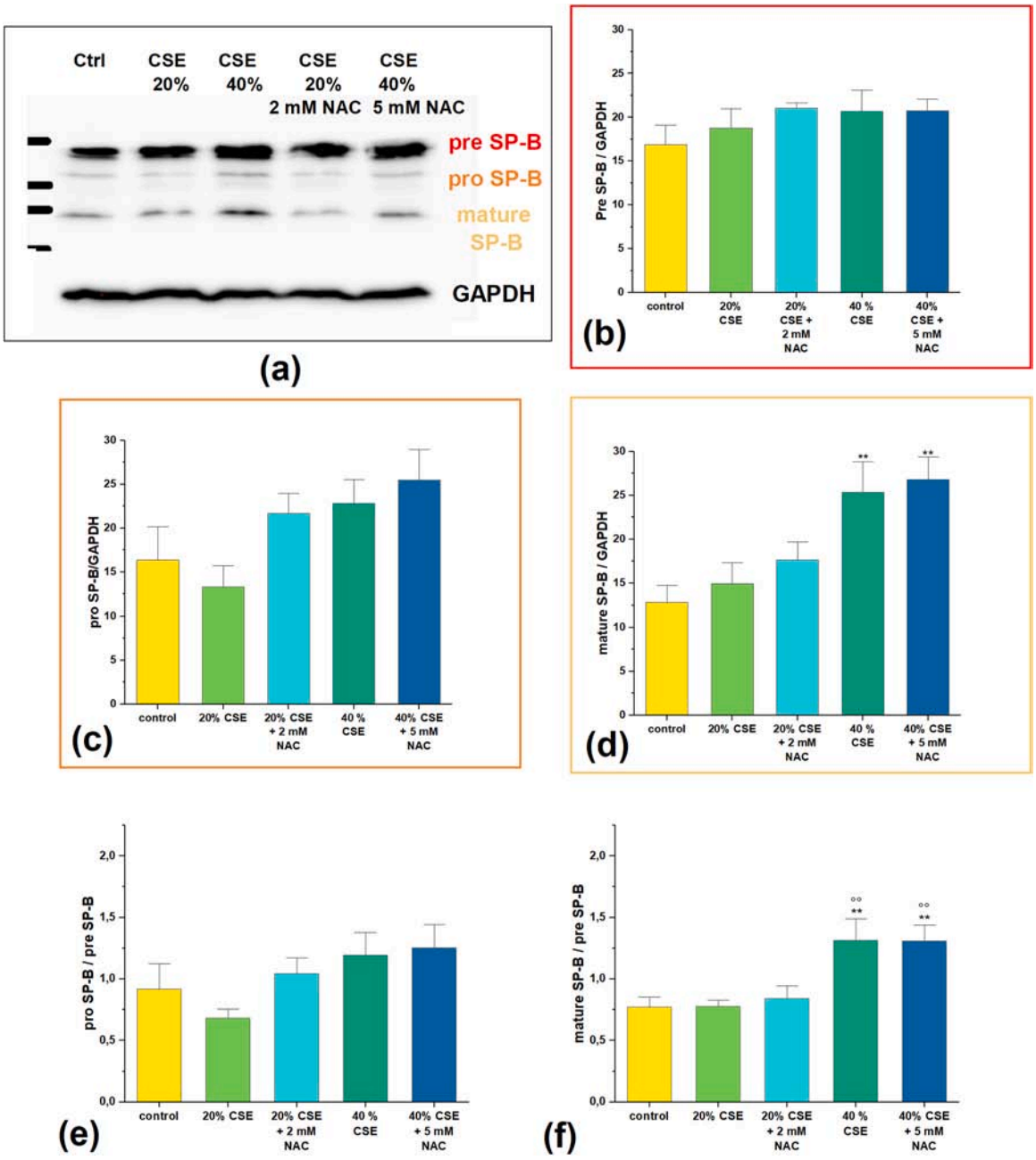

Fig. 7. Effect of CSE on intracellular SP-B levels in A549/ATII-like cells. A) Representative Western blot image showing the pre-SP-B and pro-SP-B proteins, the mature SP-B dimer, and GAPDH as a loading control. A549/ATII-like cells were exposed to 20 % or 40 % CSE, with or without NAC. The molecular weight markers on the left correspond to 37, 25 and 20, 15 kDa, respectively. B) Densitometric analysis of the pre-SP-B/GAPDH, C) pro-SP-B/GAPDH, and D) mature SP-B/GAPDH bands. E) and F) Relative quantification of the pro SP-B and the mature SP-B normalized to the pre-SP-B isoform. Data are presented as mean ± SEM. ** = $p < 0.01$ compared to control. °° = $p < 0.01$ compared to 20 % CSE (n = 6), one-way ANOVA test.

alterations in humans or animal models. This topic has been evaluated in few studies with heterogeneous results, due to anatomical and technical limitations that make this analysis complex (Garavaglia et al., 2023).

The experiments presented here were conducted on the human lung carcinoma epithelial cell line A549 differentiated into an alveolar type II (ATII)-like phenotype under appropriate growth conditions (Cooper et al., 2016). A549-ATII-like cells showed a phenotype and gene expression more similar to primary ATII cells than native A549 cells, with a significant downregulation of genes involved in cell division and up-regulation of genes involved in autophagy, differentiation, and lipidogenic pathways. Indeed, the long term culture of cells in Ham's F12, rather than standard D-MEM, led to a higher lipid accumulation within MLBs, accompanied by a marked reduction in surface tension at the air-liquid interface (figure S2 and S3). While primary human ATII cells may represent a most physiologically relevant model, their limited availability and technical challenges require the use of alternative models. A549/ATII-like cells, despite not fully replicating the characteristic of primary ATII cells, may offer a widely accessible model for preliminary mechanistic studies.

As a model for cigarette smoke exposure, we used an extract of mainstream cigarette smoke in an aqueous medium (Cigarette Smoke Extract; CSE), a method extensively used to study the effects of soluble constituents of cigarette smoke on cultured cells (Gellner et al., 2016). Despite the loss of the most volatile and reactive components, CSE reflects in vivo exposure conditions under which alveolar cells interact with smoke constituents solubilized into biological fluids (Rennard,

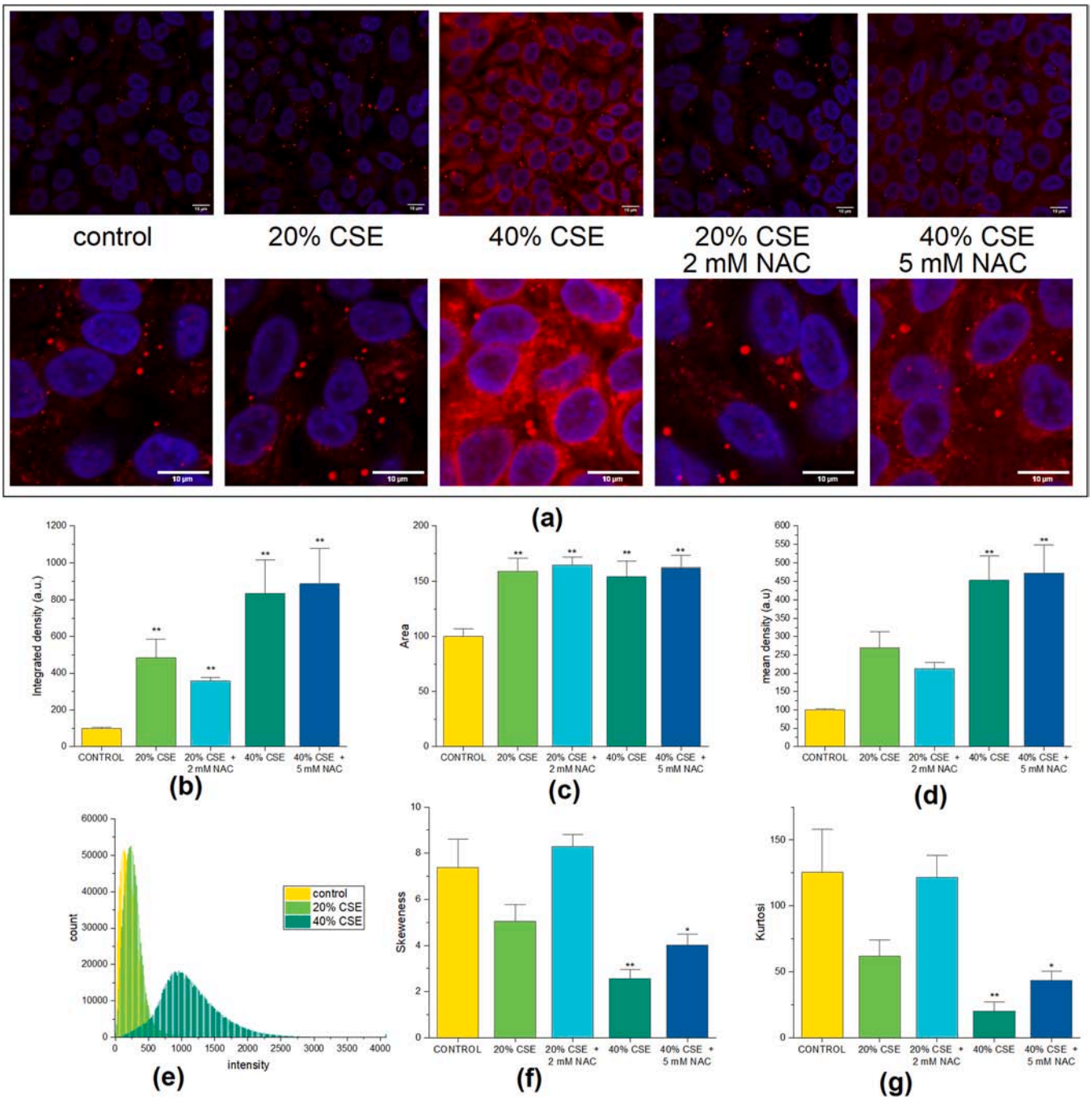

Fig. 8. Effect of CSE on the intracellular SP-B levels in A549/ATII-like cells. A) Representative confocal images acquired at 60x magnification (top row) and detailed views of the same images (bottom row). In these last images, the brightness and contrast were enhanced post-acquisition to highlight the protein distribution within the cells. Scale bar = 10 μm B) Semi-quantitative analysis of the total fluorescence intensity. C) Average area and D) signal intensity of fluorescent signal in the immunofluorescence images. E) Pixel intensity distribution for the images shown in panel A). F) Skewness and G) kurtosis of the fluorescence intensity distribution. Three independent experiments were done (total images: 15, 15, 12, 9, and 11 for control, 20 % CSE, 40 % CSE, 2 mM NAC + 20 % CSE, and 5 mM NAC + 40 % CSE, respectively). Data are presented as mean ± SEM. *, ** = $p < 0.05$, 0.01 compared to control with one-way ANOVA (post-test Bonferroni), except for panel B) where a non-parametric Kruskal-Wallis ANOVA (post-test Dunnett) was used to compare data (normality rejected by the Kolmogorv-Smirnov test).

2004).

It is well established that cigarette smoke has a cytotoxic effect on A549 alveolar cells (Hoshino et al., 2001; Takano et al., 2012; Zhang et al., 2017), leading to a reduction in cell viability.

To avoid confounding effects caused by CSE-induced cytotoxicity, we assessed the effects of increasing doses of CSE on cell viability and number in our experimental conditions, and selected 20 % and 40 % CSE concentration to perform our experiments, to preserve cell viability.

A well-known effect of cigarette smoke exposure is the induction of oxidative stress, which can alter several cellular processes (Cha et al., 2023; van der Vaart, 2004; Wang et al., 2019). Consistently, 20 % and 40 % CSE exposure induced protein carbonylation in A546/ATII-like cells (Fig. 2), confirming that CSE-mediated oxidative stress impacts intracellular proteins and may lead to functional alterations at the cellular level. This increase, in agreement with previous results in other cell lines (England et al., 2004; Messier et al., 2013; Zhao et al., 2024; Zhitkovich, 2019), was significantly reduced in the presence of the antioxidant and reducing agent NAC, that was therefore used in

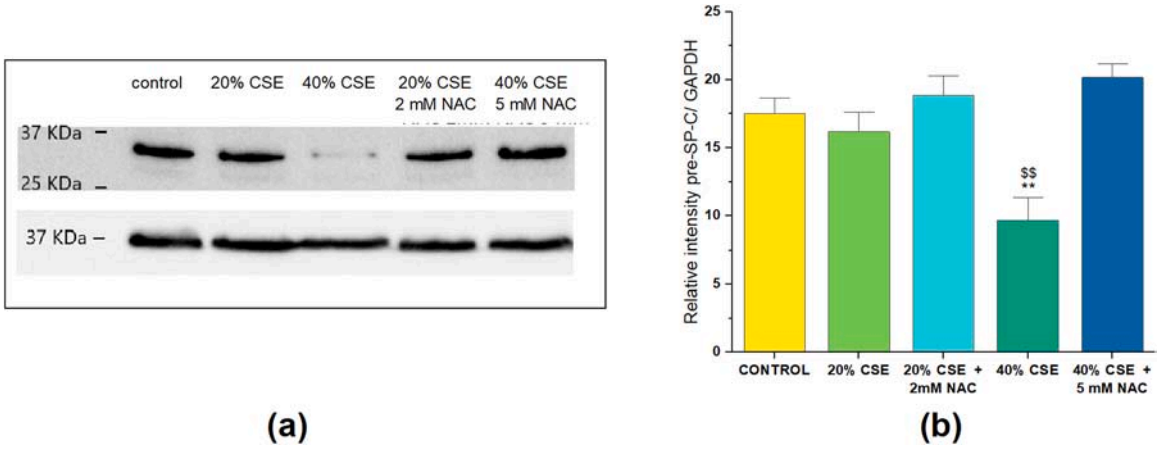

Fig. 9. Effect of CSE on the intracellular pro-SP-C expression in A549/ATII-like cells. A) Representative Western blot image showing pre-SP-C and GAPDH (as a loading control), following exposure of A549/ATII-like cells to 20 % or 40 % CSE, with or without NAC. B) Densitometric analysis of pre-SP-C/GAPDH bands. Data are presented as mean ± SEM. ** = $p < 0.01$ compared to control; $$ = $p < 0.01$ compared to 40 % CSE + 5 mM NAC (n = 7), with one-way ANOVA (post-test Bonferroni).

subsequent experiments to determine whether CSE effects on surfactant components were dependent on oxidative damage.

Effects of CSE on neutral lipid content and multilamellar body morphology were assessed using Oil Red O (ORO) staining. Spectrophotometric quantification showed that CSE exposure reduced intracellular neutral lipid levels (Fig. 3a): the effect was already significant after 20 % CSE exposure and was reversed by NAC.

Immunocytochemical image analysis showed that 40 %, but not 20 % CSE exposure, significantly decreased the number of MLBs without affecting their size (Fig. 3). This suggests that higher CSE concentration, not only limits the accumulation of neutral lipids, but also alters the maturation or degradation of the MLBs themselves. The observed reduction in neutral lipid contents could impair MLB turnover and function, reducing their capacity to store and release surfactant components, and affecting alveolar homeostasis. Although the concentration of neutral lipids in MLBs is low (Castillo-Sánchez et al., 2021; Garavaglia et al., 2023), they influence the structural organization of surfactant, thus affecting its surface activity (Discher et al., 1999; Yu and Possmayer, 1996).

The effect on neutral lipid content and MLBs was reversed by the presence of 5 mM NAC (Fig. 4), implying the involvement of oxidative stress. Additional studies using antioxidants with mechanisms of action distinct from that of NAC or pro-oxidant, such as H_2O_2, could help to confirm this hypothesis. Furthermore, future ultrastructural analysis via TEM would be useful to directly visualize CSE-induced morphological alterations in MLBs.

Our results contrast with those of Takano et al. (Takano et al., 2012), who reported an increase in both the number and size of lamellar bodies following CSE exposure in undifferentiated A549 cells. This discrepancy may arise from the fact that differences in culture conditions can significantly influence cellular responses to toxic stimuli, as more differentiated phenotypes may exhibit distinct reaction patterns (Cooper et al., 2016; Gohlsch et al., 2019; Loret et al., 2016). In agreement with our findings, cigarette smoke exposure is known to reduce levels of ATP-binding cassette transporter A3 (ABCA3), a membrane marker of MLBs (Zhang et al., 2022), and oxidative stress has been shown to cause structural degenerative modifications of these organelles (Jain et al., 1992).

Additional studies should analyze the oxidative stress-related molecular mechanism that induces the reduction in neutral lipid content and MLBs. For example, it would be worth analyzing whether CSE induced oxidative stress impairs intracellular lipid accumulation due to reduced ABCA3 expression.

A significant increase in mature SP-B levels was observed by Western blot after exposure to 40 % CSE, and this effect was not reversed by NAC. Immunofluorescence confirmed this finding and revealed a significant increase in SP-B expression also at 20 % CSE. To assess the changes in intracellular distribution of SP-B protein following exposure to CSE, image analysis was performed evaluating the skewness and kurtosis of the pixel intensity distribution. A general decrease in both indices was observed, in agreement with a more uniform distribution of the SP-B protein and reduced presence of MLB spots, where the mature protein is normally accumulated. A similar diffuse protein distribution pattern has been reported for the immature SP-B precursors in previous studies (Korimilli et al., 2000). Since evidence suggests that the final processing of the 9 kDa SP-B intermediate to the 8 kDa fully mature SP-B protein occurs in a post-Golgi compartment corresponding to the MVBs (Banfi and Agostoni, 2016; Brasch et al., 2004; Korimilli et al., 2000; Osanai et al., 2020), we hypothesize that the protein could be accumulated into the cytoplasm without reaching the MLB compartment. This interpretation is in agreement with both the increased levels of low molecular weight SP-B forms observed in Western blot and the more diffuse perinuclear fluorescence pattern corresponding to the 9 kDa precursor (Korimilli et al., 2000).

The increase in SP-B expression observed by immunofluorescence after 20 % CSE exposure was not detected by Western blot, probably because of the greater sensitivity of immunofluorescence to spatial redistribution within the cell. Notably, the alteration induced by 20 % CSE correlated with a significant rise in surface tension, suggesting that changes in SP-B localization alone may be sufficient to impair surfactant function.

Importantly, NAC did not restore SP-B localization and expression, supporting the hypothesis that oxidative stress is not the sole mechanism involved.

Previous literature reported conflicting results regarding the impact of cigarette smoke on SP-B expression (Garavaglia et al., 2023). While some showed increased SP-B mRNA in A549 cells (George et al., 2013; Takano et al., 2012), others reported reduced SP-B levels in the bronchoalveolar lavage fluid (BALF) from animal models and COPD patients (Subramaniam et al., 1996; Sun et al., 2022; Wang et al., 2021). These discrepancies may reflect differences in experimental models and exposure conditions. In agreement with the observation of Subramaniam et al. (Subramaniam et al., 1996), who reported decreased SP-B levels in BAL but not in lung tissue, our findings help clarify these seemingly conflicting results by supporting the hypothesis that intracellular accumulation of SP-B, likely due to impaired trafficking, may underlie reduced secretion, even in the presence of increased intracellular levels, ultimately contributing to the observed rise in surface

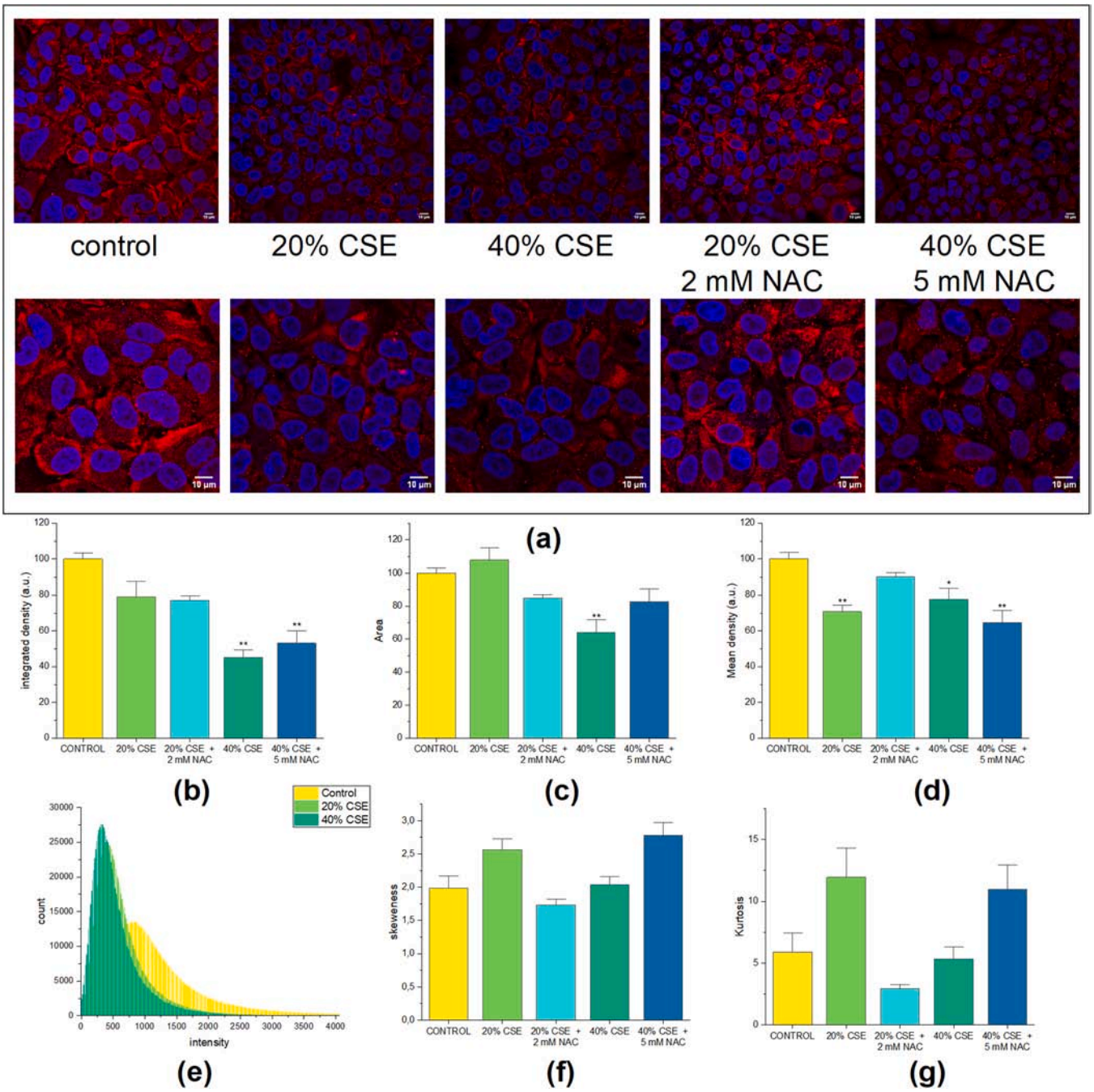

Fig. 10. Effect of CSE on the intracellular pro-SP-C levels in A549/ATII-like cells. A) Representative confocal images at 60x magnification (top row) and detailed views of the same images (bottom row). Scale bar = 10 µm. B) Total fluorescence intensity, C) mean area, and D) mean signal intensity of the confocal images. E) Pixel intensity distribution for the images shown in panel A). F) Skewness and G) kurtosis of the fluorescence intensity distribution obtained from the confocal image analysis. Three independent experiments were done, with a total of 14, 14, 12, 9, and 11 images for control, 20 % CSE, 40 % CSE, 2 mM NAC + 20 % CSE, and 5 mM NAC + 40 % CSE, respectively. Data are presented as mean ± SEM. *, ** = $p < 0.05$, 0.01 compared to control, with the one-way ANOVA test.

tension. Further studies are needed to confirm this hypothesis.

Regarding SP-C, 40 % CSE exposure resulted in a significant reduction in pro-SP-C expression, observed by both Western blot and immunofluorescence experiments. This effect was reversed by treatment with 5 mM NAC, suggesting a greater dependency for SP-C alterations on oxidative stress. This differential sensitivity between SP-B and SP-C may reflect their distinct biosynthetic pathways and structural features. In particular, SP-C contains cysteine residues, highly susceptible to oxidative modifications, critical for its processing and trafficking, whose deletion impair ER-to-Golgi transport, and promote ER stress or misfolding (Kabore et al., 2001).

Few studies have examined the effect of cigarette smoke on SP-C intracellular levels (Garavaglia et al., 2023). In agreements with our results, the expression of Pro-SP-C was reduced in the lung tissues of rats exposed to cigarette smoke and in the BALF of COPD smokers, compared to healthy non-smokers (Sun et al., 2022), as well as in primary type II alveolar cell cultures after CSE exposure (Puthusseri et al., 2017). Furthermore, oxidative stress induced by chemical agents in MLE-12 cells significantly reduced pro-SP-C expression, supporting the redox sensitivity of this protein (Bai et al., 2016).

Since one of the main surfactant functions is the reduction of surface tension, we evaluated the effect of CSE on the surface-active properties

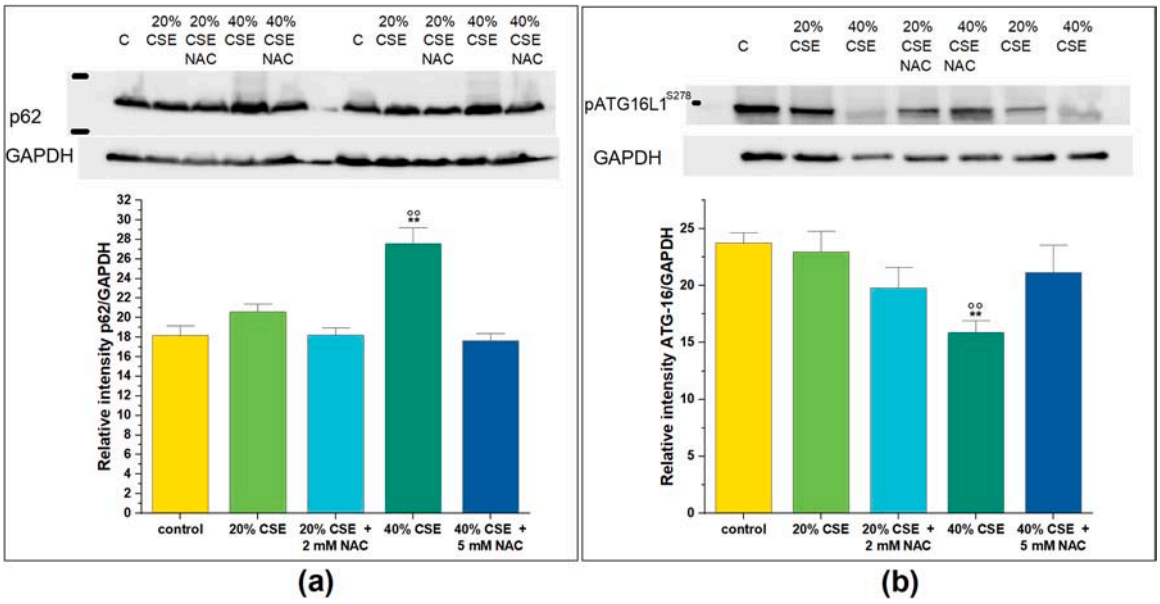

Fig. 11. Effect of CSE on the intracellular p62 and pATG16-L1^{S278} expression in A549/ATII-like cells. A) Representative Western blot showing the p62 and GAPDH bands in A549/ATII-like cells exposed to 20 % or 40 % CSE, with or without NAC. Molecular weight markers (75 and 50 kDa) are indicated on the left. GAPDH was used as the loading control. Lower panel: densitometric analysis of the p62/GAPDH bands, with relative quantification. B) Representative Western blot showing the pATG-16L1^{S278} and GAPDH bands following exposure of A549/ATII-like cells to 20 % or 40 % CSE, with or without NAC. Molecular weight marker (75 kDa) is indicated on the left. GAPDH was used as the loading control. GAPDH Western blot was made on the same membrane after stripping and reprobing. SDS-PAGE was performed under denaturing, reducing conditions. Lower panel: densitometric analysis of the pATG-16L1^{S278}/GAPDH bands, with relative quantification. Data are presented as mean ± SEM. ** = $p < 0.01$ compared to control; °° = $p < 0.01$ compared to 40 % CSE + 5 mM NAC, with the one-way ANOVA test (n = 7 for all conditions except for 40 % CSE + 5 mM NAC, where n = 6).

of the surfactant secreted by A549/ATII-like cells. Functionally, CSE exposure increased the surface tension at the air-liquid interface (Fig. 5). The effect was significant already after 20 % CSE exposure and not mitigated by NAC treatment.

It is important to highlight that, in our study, the observed effect cannot be ascribed to a direct interaction of CSE with the surfactant components (Bringezu et al., 2003; Cook and Webb, 1966; Higenbottam, 1989; Schmekel et al., 1992; Stenger et al., 2009), because the CSE-containing medium was removed and substituted after three hours of treatment and surfactant activity was measured after additional 24 h of culture, allowing for the production and secretion of new surfactant components before surface tension was measured. This makes a direct chemical interaction unlikely. Even if NAC treatment demonstrates a protective effect on MLB formation and intracellular neutral lipid content following CSE exposure (Fig. 4), it does not prevent the increase in surface tension (Fig. 5). The persistency of this functional impairment in the presence of NAC suggests the involvement of other mechanisms beyond oxidative stress, such as altered expression, trafficking, or recycling of the hydrophobic surfactant proteins SP-B, which is essential for proper surfactant organization, spreading and function (Johansson and Curstedt, 1997; Pérez-Gil, 2008; Serrano and Pérez-Gil, 2006; Weaver, 1998; Weaver and Conkright, 2001).

Interestingly, we do not observe a reduction in the extracellular levels of PC, the major surface-active component of the surfactant (Fig. 6), in agreement with previous studies reporting that PC levels often are unchanged, despite cigarette smoke-induced alteration of the total lipid content and composition of surfactant (Garavaglia et al., 2023).

The discrepancy between unchanged PC levels and reduced intracellular MLBs may suggest a possible impairment in surfactant reuptake. CSE may disrupt the recycling of phospholipids, leading to intracellular MLB depletion while maintaining extracellular PC. Since SP-C is also known to enable the uptake of surfactant phospholipids into ATII cells (Johansson, 1998; Wert et al., 2009), the reduction of SP-C expression observed in our experiments could impair the PC reuptake, further supporting this hypothesis.

Future studies should investigate the effect of CSE on the MLBs fusion dynamics, exocytosis, and surfactant reuptake using advanced imaging and biochemical methods (Haller et al., 1998).

Several molecular mechanisms could mediate the effect of CSE, such as the alteration in protein processing or in vesicular trafficking (Cheng et al., 2022; Chiappara et al., 2022; Somborac-Bačura et al., 2013; Wang et al., 2022; Wasnick et al., 2023).

Among the molecular mechanisms affected by CSE that could influence surfactant production, recent studies analyzed the effect of CSE on autophagy, a process required for MLBs formation and surfactant homeostasis in the lung (Hariri et al., 2000; Li et al., 2022; Morishita et al., 2020, 2021; Weaver et al., 2002). However, published findings are often contrasting, showing either activation (An et al., 2012; Chen et al., 2008) or inhibition of the autophagic flux (Kono et al., 2021; Li et al., 2022; Zhang et al., 2021). As autophagy shows a complex interaction with oxidative stress (Lin et al., 2024; Ornatowski et al., 2020) and is known to be altered by cigarette smoke exposure (Akhtari et al., 2024; Racanelli et al., 2018), we analyzed the effect of CSE on this pathway and, in particular, we evaluated the effects of CSE on the autophagy-related 16-like 1 (ATG16-L1) protein phosphorylated on the serine 278 (pATG16-L1^{s278}), a marker of autophagy induction, to clarify whether autophagy is impaired or activated. We also studied p62/SQSTM1 protein levels and its colocalization with pATG16L1^{s278} to confirm potential alterations in autophagosome formation.

pATG16-L1^{s278} is involved, with other proteins, in the early stages of autophagosome formation, promoting the conjugation of phosphatidylethanolamine (PE) to LC3B (Gammoh, 2020; Lystad et al., 2019). The phosphorylation on serine 278 is considered a marker of the early stages of autophagy induction (Fujii et al., 2012; Ryter and Choi, 2010). Since autophagy is primarily modulated via post-translational mechanisms such as phosphorylation, we focused on this activated form rather than total ATG16L1 levels.

p62/SQSTM1 is a well-known autophagic cargo receptor that binds to both the substrates and the autophagosomal membrane protein LC3

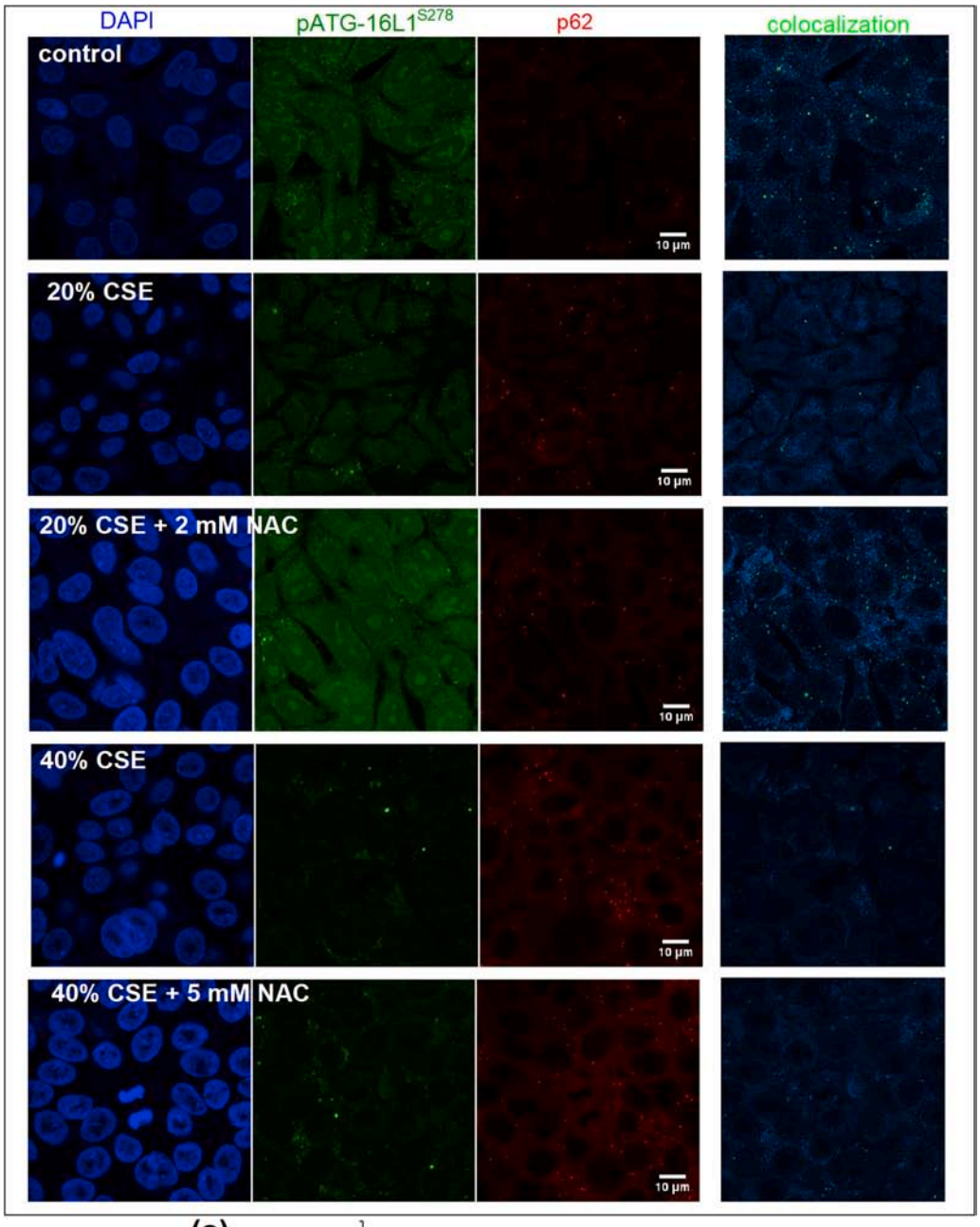

(caption on next page)

Fig. 12. Effect of CSE on p62 and pATG-16L1^{S278} localization in A549/ATII-like cells. A) Representative confocal laser scanning microscopy images of double-labelled immunofluorescence for nuclei (DAPI), pATG-16L1^{S278} (green, Cy2 fluorescence), and p62 (red, Cy5 fluorescence). To minimize crosstalk, channels were acquired sequentially. The right column displays computationally generated images, using the logical "AND" function and a "green-red-blue" lookup table to highlight the regions of signals colocalization. Higher-intensity regions, where both signals co-occur, are shown in green. B) Quantitative analysis of the colocalization area of p62 and pATG16L1^{S278} signals under different experimental conditions. Data are presented as mean ± SEM. ** = $p < 0.01$ compared to control with the one-way ANOVA test (n = 8 in control and n = 5 after CSE or CSE and NAC exposure).

(Huang et al., 2024). Moreover, p62 links autophagy to the Nrf2-Keap1-ARE axis (Jiang et al., 2015), activating cytoprotective genes and contributing to the cellular response to oxidative stress and xenobiotics, such as environmental pollutants and harmful chemicals. The evaluation of p62 in this study provides a foundation for further analysis of its role in these interconnected cellular processes.

Western blot experiments showed (Fig. 11) a significant increase in p62 protein levels and a decrease in pATG16-L1^{s278} expression when cells were exposed to 40 % CSE, indicating inhibition of early autophagy initiation. Colocalization between these markers also decreased, further suggesting a block in autophagosome formation. While expression level modifications of the two proteins were NAC-reversible, the reduction in colocalization was not, implying that some unidentified molecular pathways, influenced by CSE and modulating autophagy, are resistant to antioxidant treatment. Moreover, besides its antioxidant effect, NAC itself may inhibit autophagy via mTOR activation and AMPK inhibition (Kim et al., 2020; Lin et al., 2020; Sano et al., 2019; Wang et al., 2021; Wang et al., 2017), potentially limiting its effect to restore surfactant function.

To our knowledge, no previous studies evaluated the direct connection between the expression of the phospho-activated pATG16-L1^{s278} and cigarette smoke exposure. Accumulation of p62 in lungs of smokers (Bodas et al., 2019; Vij et al., 2018), along with our data, provide mechanistic insights linking these findings to surfactant dysfunction. Accumulation of p62 and impaired autophagy have been reported both in cell line, murine model and the lungs of smokers (Bodas et al., 2019; Tran et al., 2015; Vij et al., 2018). Our findings, demonstrating that CSE does not activate autophagy, but rather impair its early initiation stage, suggest potential mechanisms linking the observation of the existing literature to surfactant dysfunction.

The principal results of this study are summarized in Fig. 13.

Taken together, our results suggest that impaired autophagy may contribute to defective MLB maturation and SP-B processing, leading to intracellular accumulation and decreased surfactant secretion, in agreement with other studies (Subramaniam et al., 1996). This could explain the rise of surface tension.

While our findings contribute to the understanding of the acute effects of CSE on surfactant production by ATII cells, some methodological and biological limitations need to be evidenced.

Although the A549/ATII-like cell model exhibits several features of ATII cells, it does not fully replicate the complexity of the alveolar environment in vivo, where various resident lung cells (e.g., macrophages, fibroblasts) and mechanical forces contribute to surfactant production and secretion. Additional research using more complex model systems, such as lung organoids or in vivo analysis, should be employed to confirm our observations.

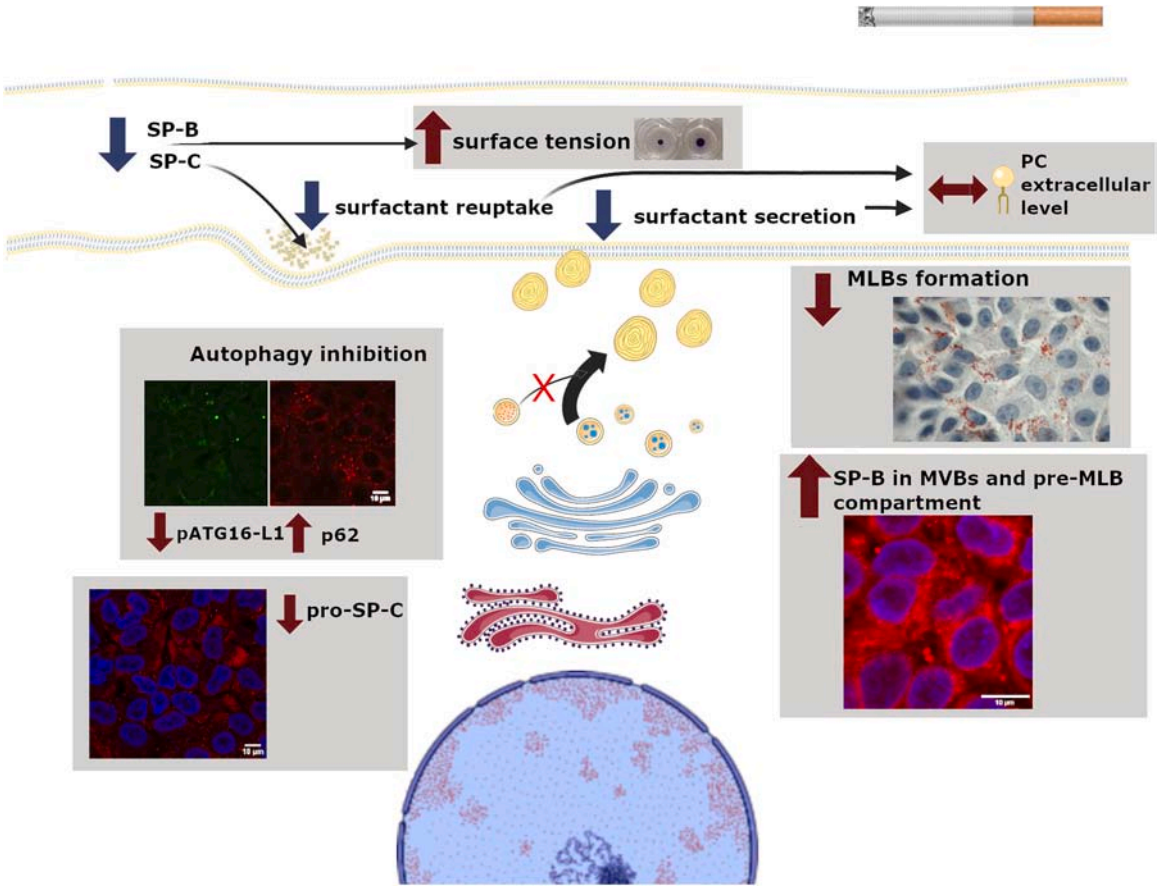

Fig. 13. Schematic representation of the CSE-induced alterations in A549/ATII-like cells, experimentally confirmed (red arrows) or hypothesized on the basis of literature analysis (blue arrows). The brightness of images in the "autophagy inhibition" box has been enhanced to make them visible.

Furthermore, we did not analyze the post-translational modifications that may alter surfactant protein function. Mass spectrometry analysis can be used to study these post-translational changes in more detail. This method could be used to analyze variation in surfactant lipid composition.

Beyond oxidative stress and autophagy early step disruption, CSE may also affect other intracellular pathways. These include inflammatory mediators (e.g., IL-6, TNF-α), ER stress inducing unfolded protein response (UPR), and epigenetic modifications, such as CSE-induced DNA methylation and histone modifications, all of which can impair ATII cell differentiation and surfactant metabolism (Carroll et al., 2002; Laganà et al., 2020; Lawson et al., 2008; Mason and Voelker, 1998; Zhong et al., 2011; Zong et al., 2019). Studies on these mechanisms by means of RNA sequencing, proteomic analysis, and inflammatory marker quantifications will be necessary in the future to elucidate the pathways involved in CSE-induced surfactant dysfunction.

Another relevant mechanism is the CSE-induced increase in intracellular calcium levels, observed in A549 and other lung cell models (Dabo et al., 2024; (YOO et al., 2020). Cytosolic Ca^{2+} dysregulation is known to contribute to oxidative stress (Rodríguez-Pérez et al., 2025), apoptosis (Ermak and Davies, 2002), and autophagy (Sukumaran et al., 2021), thereby potentially affecting surfactant production or secretion. Although not directly assessed in this study, future experiments using calcium-sensitive dyes such as Fluo-4/AM and real-time imaging would be essential to explore these mechanisms.

Our study highlights an early and specific disruption of surfactant function following smoke exposure. The alterations observed in surfactant properties —namely, increased surface tension and altered SP-B/SP-C balance— although derived from an acute exposure model, may have mechanistic implications for pulmonary function, related to lung disease development.

A significant association between smoking and an increased risk of ARDS has been evidenced (Zhang et al., 2024). Although ARDS-related observed clinical alteration are not limited to surfactant, extensive animal studies and several human reports have shown an alteration of the lipidomic profile with a functionally relevant alteration of neutral lipid (Markart et al., 2007) and with decreased levels of SP-B and SP-C in bronchoalveolar lavage (BAL) samples (Gregory et al., 1991; Günther et al., 1996; Savani et al., 2001). Furthermore, the surface tension–lowering properties of the isolated surfactant are abnormal (Gregory et al., 1991; Petty and Ashbaugh, 1971). These abnormalities correlated with the severity of ARDS.

Cigarette smoking is related to worse asthma outcomes for several clinical and functional respiratory variables, compared to never smoking (Huang et al., 2023). Even if the variable and reversible airways obstruction observed in asthma, due to airway inflammation and bronchial hyperresponsiveness, is predominantly caused by smooth muscle constriction, mucosal oedema and secretion of fluid into the airway lumen, several reports demonstrate that this effect may partly be due to a poor function of pulmonary surfactant (Hohlfeld, 2001), a known factor involved in the regulation of airway calibres and a modulator of allergic inflammation. Therefore, the observed surfactant impairment induced by smoke exposure may be related to the aggravation of asthma outcomes in cigarette smokers, along with the cigarette smoke-induced alteration of airways inflammation phenotypes and remodelling (Huang et al., 2023).

Although our model reflects acute exposure, these early changes in surfactant composition and function may reflect the initial molecular events that, under conditions of repeated or sustained insult (e.g., chronic smoking), contribute to persistent surfactant dysfunction. In fact, similar surfactant abnormalities—including elevated surface tension and decreased SP-B levels—have been reported in clinical studies performed on smokers with early-stage COPD (Hohlfeld et al., 1997; Hristova et al., 2021; Zhao et al., 2010). Moreover, in IPF (idiopathic pulmonary fibrosis) ATII dysfunction and lamellar body defects have been described (Birkelbach et al., 2015), as well as abnormalities of lung surfactant leading to a decreased surface tension lowering ability (Devendra and Spragg, 2002). The acute surfactant impairment observed in our study may represent therefore a precursor state, potentially contributing to the pathogenesis of smoking-related pulmonary diseases if left unresolved. The imbalance between SP-B and SP-C and the elevated surface tension observed in our model could mimic the early molecular changes that contribute to alveolar instability and impaired gas exchange leading to chronic lung remodelling commonly seen in these diseases. Further supporting this, mutations in the SFTPB and SFTPC genes are known causes of familial interstitial lung diseases, highlighting the importance of these proteins in maintaining lung homeostasis (Amin et al., 2001; Desroziers et al., 2023; Nogee et al., 2002, 2001).

In conclusion, this study demonstrates a direct effect of CSE on the expression of surfactant components (such as neutral lipids, SP-B, and SP-C) in A549/ATII-like cells, with functional consequences on the surface activity of the surfactant, via oxidative stress-dependent and independent mechanisms. Autophagy impairment, particularly at the initiation phase, contributes to altered SP-B processing and MLB dysfunction. NAC can partially mitigate cigarette smoke-induced lung injury via antioxidant mechanisms. However, its inhibitory effect on early autophagy signaling (via AMPK/mTOR) may limit the protective effect on surfactant components and function. Autophagy enhancing therapeutic agents, either alone or in association with NAC, may be effective to correct cigarette smoke-induced autophagy dysfunction.

Funding

This research received no external funding.

CRediT authorship contribution statement

Chiara Sironi: Writing – review & editing, Methodology, Investigation, Formal analysis, Data curation. **Francesca Bodega:** Writing – review & editing, Writing – original draft, Visualization, Validation, Supervision, Methodology, Investigation, Funding acquisition, Formal analysis, Data curation, Conceptualization. **Isabella Dalle-Donne:** Writing – review & editing, Supervision, Funding acquisition. **Cristina Porta:** Writing – review & editing, Supervision, Funding acquisition, Formal analysis, Conceptualization. **Maria Lisa Garavaglia:** Writing – review & editing, Writing – original draft, Visualization, Validation, Methodology, Investigation, Formal analysis, Data curation, Conceptualization.

Declaration of Competing Interest

The authors declare that they have no known competing financial interests or personal relationships that could have appeared to influence the work reported in this paper.

Appendix A. Supporting information

Supplementary data associated with this article can be found in the online version at doi:10.1016/j.tox.2025.154262.

Data availability

Data will be made available on request.

References

Adatia, A., Wahab, M., Shahid, I., Moinuddin, A., Killian, K.J., Satia, I., 2021. Effects of cigarette smoke exposure on pulmonary physiology, muscle strength and exercise capacity in a retrospective cohort with 30,000 subjects. PLoS One 16, e0250957. https://doi.org/10.1371/journal.pone.0250957.

Agraval, H., Sharma, J.R., Yadav, U.C.S., 2022. Method of preparation of cigarette smoke extract to assess. Lung CancerAssoc. Chang. Airw. Epithel. Cells 121–132. https://doi.org/10.1007/978-1-0716-1896-7_13.

Akhtari, M., Jalalvand, M., Sadr, M., Sharifi, H., 2024. Autophagy in the cellular consequences of tobacco smoking: insights into senescence. J. Biochem Mol. Toxicol. 38. https://doi.org/10.1002/jbt.70065.

Albano, G.D., Montalbano, A.M., Gagliardo, R., Profita, M., 2023. Autophagy/Mitophagy in airway diseases: impact of oxidative stress on epithelial cells. Biomolecules 13, 1217. https://doi.org/10.3390/biom13081217.

Amin, R.S., Wert, S.E., Baughman, R.P., Tomashefski, J.F., Nogee, L.M., Brody, A.S., Hull, W.M., Whitsett, J.A., 2001. Surfactant protein deficiency in familial interstitial lung disease. J. Pedia 139, 85–92. https://doi.org/10.1067/mpd.2001.114545.

An, C.H., Wang, X.M., Lam, H.C., Ifedigbo, E., Washko, G.R., Ryter, S.W., Choi, A.M.K., 2012. TLR4 deficiency promotes autophagy during cigarette smoke-induced pulmonary emphysema. Am. J. Physiol. Lung Cell. Mol. Physiol. 303, L748–L757. https://doi.org/10.1152/ajplung.00102.2012.

Bai, R., Guan, L., Zhang, W., Xu, J., Rui, W., Zhang, F., Ding, W., 2016. Comparative study of the effects of PM1-induced oxidative stress on autophagy and surfactant protein b and c expressions in lung alveolar type II epithelial MLE-12 cells. Biochim. Et. Biophys. Acta (BBA) Gen. Subj. 1860, 2782–2792. https://doi.org/10.1016/j.bbagen.2016.05.020.

Banfi, C., Agostoni, P., 2016. Surfactant protein B: from biochemistry to its potential role as diagnostic and prognostic marker in heart failure. Int J. Cardiol. 221, 456–462. https://doi.org/10.1016/j.ijcard.2016.07.003.

Bernhard, W., 2016. Lung surfactant: function and composition in the context of development and respiratory physiology. Ann. Anat. Anat. Anz. 208, 146–150. https://doi.org/10.1016/j.aanat.2016.08.003.

Birkelbach, B., Lutz, D., Ruppert, C., Henneke, I., Lopez-Rodriguez, E., Günther, A., Ochs, M., Mahavadi, P., Knudsen, L., 2015. Linking progression of fibrotic lung remodeling and ultrastructural alterations of alveolar epithelial type II cells in the amiodarone mouse model. Am. J. Physiol. Lung Cell. Mol. Physiol. 309, L63–L75. https://doi.org/10.1152/ajplung.00279.2014.

Blank, F., Rothen-Rutishauser, B.M., Schurch, S., Gehr, P., 2006. An optimized in vitro model of the respiratory. Trac. Wall Study Part. Cell Interact. 19, 392–405. https://doi.org/10.1089/JAM.2006.19.392. ⟨http://www.liebertpub.com/jam⟩.

Bodas, M., Pehote, G., Silverberg, D., Gulbins, E., Vij, N., 2019. Autophagy augmentation alleviates cigarette smoke-induced CFTR-dysfunction, ceramide-accumulation and COPD-emphysema pathogenesis. Free Radic. Biol. Med 131, 81–97. https://doi.org/10.1016/j.freeradbiomed.2018.11.023.

Boo, H.-J., Min, H.-Y., Park, C.-S., Park, J.-S., Jeong, J.Y., Lee, S.Y., Kim, W.-Y., Lee, J.-W., Oh, S.-R., Park, R.-W., Lee, H.-Y., 2023. Dual impact of IGF2 on alveolar stem cell function during Tobacco-Induced injury repair and development of pulmonary emphysema and cancer. Cancer Res 83, 1782–1799. https://doi.org/10.1158/0008-5472.CAN-22-3543.

Brasch, F., Johnen, G., Winn-Brasch, A., Guttentag, S.H., Schmiedl, A., Kapp, N., Suzuki, Y., Müller, K.M., Richter, J., Hawgood, S., Ochs, M., 2004. Surfactant protein b in type II pneumocytes and intra-alveolar surfactant forms of human lungs. Am. J. Respir. Cell Mol. Biol. 30, 449–458. https://doi.org/10.1165/rcmb.2003-0262OC.

Bringezu, F., Pinkerton, K.E., Zasadzinski, J.A., 2003. Environmental tobacco smoke effects on the primary lipids of lung surfactant. Langmuir 19, 2900–2907. https://doi.org/10.1021/la026455e.

Caito, S., Rajendrasozhan, S., Cook, S., Chung, S., Yao, H., Friedman, A.E., Brookes, P.S., Rahman, I., 2010. SIRT1 is a redox-sensitive deacetylase that is post-translationally modified by oxidants and carbonyl stress. FASEB J. 24, 3145–3159. https://doi.org/10.1096/fj.09-151308.

Calafat, A.M., Polzin, G.M., Saylor, J., Richter, P., Ashley, D.L., Watson, C.H., 2004. Determination of tar, nicotine, and carbon monoxide yields in the mainstream smoke of selected international cigarettes. Tob. Control 13, 45–51. https://doi.org/10.1136/tc.2003.003673.

Cañadas, O., Olmeda, B., Alonso, A., Pérez-Gil, J., 2020. Lipid–Protein and Protein–Protein interactions in the pulmonary surfactant system and their role in lung homeostasis. Int J. Mol. Sci. 21, 3708. https://doi.org/10.3390/ijms21103708.

Carroll, B., Otten, E.G., Manni, D., Stefanatos, R., Menzies, F.M., Smith, G.R., Jurk, D., Kenneth, N., Wilkinson, S., Passos, J.F., Attems, J., Veal, E.A., Teyssou, E., Seilhean, D., Millecamps, S., Eskelinen, E.-L., Bronowska, A.K., Rubinsztein, D.C., Sanz, A., Korolchuk, V.I., 2018. Oxidation of SQSTM1/p62 mediates the link between redox state and protein homeostasis. Nat. Commun. 9, 256. https://doi.org/10.1038/s41467-017-02746-z.

Carroll, J.L., McCoy, D.M., McGowan, S.E., Salome, R.G., Ryan, A.J., Mallampalli, R.K., 2002. Pulmonary-specific expression of tumor necrosis factor-α alters surfactant lipid metabolism. Am. J. Physiol. Lung Cell. Mol. Physiol. 282, L735–L742. https://doi.org/10.1152/ajplung.00120.2001.

Castillo-Sánchez, J.C., Cruz, A., Pérez-Gil, J., 2021. Structural hallmarks of lung surfactant: Lipid-protein interactions, membrane structure and future challenges. Arch. Biochem Biophys. 703, 108850. https://doi.org/10.1016/j.abb.2021.108850.

Centers for Disease Control and Prevention (US); National Center for Chronic Disease Prevention and Health Promotion (US); Office on Smoking and Health (US)., 2010. How tobacco smoke causes disease: the biology and behavioral basis for smoking-attributable disease: a report of the Surgeon General. U.S. Dept. of Health and Human Services, Public Health Service, Office of the Surgeon General; For sale by the Supt. of Docs., U.S. G.P.O.

Chang, C., Jensen, L.E., Hurley, J.H., 2021. Autophagosome biogenesis comes out of the black box. Nat. Cell Biol. 23, 450–456. https://doi.org/10.1038/s41556-021-00669-y.

Cha, S.-R., Jang, J., Park, S.-M., Ryu, S.M., Cho, S.-J., Yang, S.-R., 2023. Cigarette Smoke-Induced respiratory response: insights into cellular processes and biomarkers. Antioxidants 12, 1210. https://doi.org/10.3390/antiox12061210.

Cheng, Y., Gu, W., Zhang, G., Guo, X., 2022. Notch1 activation of Jagged1 contributes to differentiation of mesenchymal stem cells into endothelial cells under cigarette smoke extract exposure. BMC Pulm. Med 22, 139. https://doi.org/10.1186/s12890-022-01913-3.

Chen, Z.-H., Kim, H.P., Sciurba, F.C., Lee, S.-J., Feghali-Bostwick, C., Stolz, D.B., Dhir, R., Landreneau, R.J., Schuchert, M.J., Yousem, S.A., Nakahira, K., Pilewski, J.M., Lee, J. S., Zhang, Y., Ryter, S.W., Choi, A.M.K., 2008. Egr-1 regulates autophagy in cigarette Smoke-Induced chronic obstructive pulmonary disease. PLoS One 3, e3316. https://doi.org/10.1371/journal.pone.0003316.

Chiappara, G., Di Vincenzo, S., Sangiorgi, C., Di Sano, C., D'Anna, C., Zito, G., Cipollina, C., Vitulo, P., Bertani, A., Pace, E., 2022. Cigarette smoke upregulates Notch-1 signaling pathway and promotes lung adenocarcinoma progression. Toxicol. Lett. 355, 31–40. https://doi.org/10.1016/j.toxlet.2021.11.002.

Cipollina, C., Bruno, A., Fasola, S., Cristaldi, M., Patella, B., Inguanta, R., Vilasi, A., Aiello, G., La Grutta, S., Torino, C., Pace, E., 2022. Cellular and molecular signatures of oxidative stress in bronchial epithelial cell models injured by cigarette smoke extract. Int J. Mol. Sci. 23, 1770. https://doi.org/10.3390/ijms23031770.

Colombo, G., Clerici, M., Garavaglia, M.E., Giustarini, D., Rossi, R., Milzani, A., Dalle-Donne, I., 2016. A step-by-step protocol for assaying protein carbonylation in biological samples. J. Chromatogr. B 1019, 178–190. https://doi.org/10.1016/j.jchromb.2015.11.052.

Colombo, G., Garavaglia, M.L., Astori, E., Giustarini, D., Rossi, R., Milzani, A., Dalle-Donne, I., 2019. Protein carbonylation in human bronchial epithelial cells exposed to cigarette smoke extract. Cell Biol. Toxicol. 35, 345–360. https://doi.org/10.1007/s10565-019-09460-0.

Cook, W.A., Webb, W.R., 1966. Surfactant in chronic smokers. Ann. Thorac. Surg. 2, 327–333. https://doi.org/10.1016/S0003-4975(10)66584-8.

Cooper, J.R., Abdullatif, M.B., Burnett, E.C., Kempsell, K.E., Conforti, F., Tolley, H., Collins, J.E., Davies, D.E., 2016. Long term culture of the A549 cancer cell line promotes multilamellar body formation and differentiation towards an alveolar type II pneumocyte phenotype. PLoS One 11, e0164438. https://doi.org/10.1371/journal.pone.0164438.

Dabo, A.J., Raghavan, S., Ezegbunam, W., Thankachen, J., Evgrafov, O., Majka, S., Geraghty, P., Foronjy, R.F., 2024. Cigarette smoke alters calcium flux to induce PP2A membrane trafficking and endothelial cell permeability. Sci. Rep. 14, 28012. https://doi.org/10.1038/s41598-024-77776-x.

Dalle-Donne, I., Colombo, G., Gornati, R., Garavaglia, M.L., Portinaro, N., Giustarini, D., Bernardini, G., Rossi, R., Milzani, A., 2017. Protein carbonylation in human smokers and mammalian models of exposure to cigarette smoke: focus on redox proteomic studies. Antioxid. Redox Signal 26, 406–426. https://doi.org/10.1089/ars.2016.6772.

Dalle-Donne, I., Giustarini, D., Colombo, R., Rossi, R., Milzani, A., 2003a. Protein carbonylation in human diseases. Trends Mol. Med 9, 169–176. https://doi.org/10.1016/S1471-4914(03)00031-5.

Dalle-Donne, I., Rossi, R., Giustarini, D., Milzani, A., Colombo, R., 2003b. Protein carbonyl groups as biomarkers of oxidative stress. Clin. Chim. Acta 329, 23–38. https://doi.org/10.1016/S0009-8981(03)00003-2.

da Silva, P.F., de Matos, N.A., Ramos, C., de, O., Castro, T., de, F., Araújo, N.P., da, S., de Souza, A.B.F., Costa, G., de, P., Cangussú, S.D., Talvani, A., Nagato, A.C., Bezerra, F. S., 2022. Acute outcomes of cigarette smoke and electronic cigarette aerosol inhalation in a murine model. Biomed. Res Int 2022. https://doi.org/10.1155/2022/9938179.

Degasperi, A., Birtwistle, M.R., Volinsky, N., Rauch, J., Kolch, W., Kholodenko, B.N., 2014. Evaluating strategies to normalise biological replicates of Western blot data. PLoS One 9, e87293. https://doi.org/10.1371/journal.pone.0087293.

Desroziers, T., Prévot, G., Coulomb, A., Nau, V., Dastot-Le Moal, F., Duquesnoy, P., Héry, M., Le Borgne, A., Amselem, S., Legendre, M., Nathan, N., 2023. Hypomorphic pathogenic variant in SFTPB leads to adult pulmonary fibrosis. Eur. J. Hum. Genet. 31, 1083–1087. https://doi.org/10.1038/s41431-023-01413-w.

Deutsch, M.J., Schriever, S.C., Roscher, A.A., Ensenauer, R., 2014. Digital image analysis approach for lipid droplet size quantitation of oil red O-stained cultured cells. Anal. Biochem 445, 87–89. https://doi.org/10.1016/j.ab.2013.10.001.

Devendra, G., Spragg, R.G., 2002. Lung surfactant in subacute pulmonary disease. Respir. Res 3, 11. https://doi.org/10.1186/rr168.

Dietl, P., Frick, M., 2021. Channels and transporters of the pulmonary lamellar body in health and disease. Cells 11, 45. https://doi.org/10.3390/cells11010045.

Discher, B.M., Maloney, K.M., Grainger, D.W., Sousa, C.A., Hall, S.B., 1999. Neutral lipids induce critical behavior in interfacial monolayers of pulmonary surfactant. Biochemistry 38, 374–383. https://doi.org/10.1021/bi981386h.

Doyle, I.R., Jones, M.E., Barr, H.A., Orgeig, S., Crockett, A.J., McDonald, C.F., Nicholas, T.E., 1994. Composition of human pulmonary surfactant varies with exercise and level of fitness. Am. J. Respir. Crit. Care Med 149, 1619–1627. https://doi.org/10.1164/ajrccm.149.6.8004321.

Elisia, I., Lam, V., Cho, B., Hay, M., Li, M.Y., Yeung, M., Bu, L., Jia, W., Norton, N., Lam, S., Krystal, G., 2020. The effect of smoking on chronic inflammation, immune function and blood cell composition. Sci. Rep. 10, 19480. https://doi.org/10.1038/s41598-020-76556-7.

England, K., O'Driscoll, C., Cotter, T.G., 2004. Carbonylation of glycolytic proteins is a key response to drug-induced oxidative stress and apoptosis. Cell Death Differ. 11, 252–260. https://doi.org/10.1038/sj.cdd.4401338.

Ermak, G., Davies, K.J.A., 2002. Calcium and oxidative stress: from cell signaling to cell death. Mol. Immunol. 38, 713–721. https://doi.org/10.1016/S0161-5890(01)00108-0.

Faizan, M.I., Kaur, G., Shaikh, S.B., Effah, F., Unwalla, H., Rahman, I., 2025. Genetic diversity leads to differential inflammatory responses to cigarette smoke in mice. Physiol. Rep. 13. https://doi.org/10.14814/phy2.70199.
Feoktistova, M., Geserick, P., Leverkus, M., 2016. Crystal violet assay for determining viability of cultured cells. Cold Spring Harb. Protoc. 2016, pdb.prot087379. https://doi.org/10.1101/pdb.prot087379.
Fleischmann, M., Jarnicki, A.G., Brown, A.S., Yang, C., Anderson, G.P., Garbi, N., Hartland, E.L., van Driel, I.R., Ng, G.Z., 2023. Cigarette smoke depletes alveolar macrophages and delays clearance of *legionella pneumophila*. Am. J. Physiol. Lung Cell. Mol. Physiol. 324, L373–L384. https://doi.org/10.1152/ajplung.00268.2022.
Fröhlich, E., Mercuri, A., Wu, S., Salar-Behzadi, S., 2016. Measurements of deposition, lung surface area and lung fluid for simulation of inhaled compounds. Front Pharm. 7. https://doi.org/10.3389/fphar.2016.00181.
Fujii, S., Hara, H., Araya, J., Takasaka, N., Kojima, J., Ito, S., Minagawa, S., Yumino, Y., Ishikawa, T., Numata, T., Kawaishi, M., Hirano, J., Odaka, M., Morikawa, T., Nishimura, S., Nakayama, K., Kuwano, K., 2012. Insufficient autophagy promotes bronchial epithelial cell senescence in chronic obstructive pulmonary disease. Oncoimmunology 1, 630–641. https://doi.org/10.4161/onci.20297.
Gallucci, G., Tartarone, A., Lerose, R., Lalinga, A.V., Capobianco, A.M., 2020. Cardiovascular risk of smoking and benefits of smoking cessation. J. Thorac. Dis. 12, 3866–3876. https://doi.org/10.21037/jtd.2020.02.47.
Gammoh, N., 2020. The multifaceted functions of ATG16L1 in autophagy and related processes. J. Cell Sci. 133. https://doi.org/10.1242/jcs.249227.
Garavaglia, M.L., Bodega, F., Porta, C., Milzani, A., Sironi, C., Dalle-Donne, I., 2023. Molecular impact of conventional and electronic cigarettes on pulmonary surfactant. Int J. Mol. Sci. 24, 11702. https://doi.org/10.3390/ijms241411702.
Gellner, C.A., Reynaga, D.D., Leslie, F.M., 2016. Cigarette smoke extract: a preclinical model of tobacco dependence. Curr. Protoc. Neurosci. 77. https://doi.org/10.1002/cpns.14.
George, U.M., Ashna, U., Kumar, S.S.P., Nandkumar, A.M., 2013. Effect of tobacco extract on surfactant synthesis and its reversal by retinoic acid—role of cell–cell interactions in vitro. Vitr. Cell Dev. Biol. Anim. 49, 260–269. https://doi.org/10.1007/s11626-013-9595-3.
Ghasemi, M., Turnbull, T., Sebastian, S., Kempson, I., 2021. The MTT assay: utility, limitations, pitfalls, and interpretation in bulk and Single-Cell analysis. Int J. Mol. Sci. 22, 12827. https://doi.org/10.3390/ijms222312827.
Goerke, J., 1998. Pulmonary surfactant: functions and molecular composition. Biochim. Et. Biophys. Acta (BBA) Mol. Basis Dis. 1408, 79–89. https://doi.org/10.1016/S0925-4439(98)00060-X.
Gohlsch, K., Mückter, H., Steinritz, D., Aufderheide, M., Hoffmann, S., Gudermann, T., Breit, A., 2019. Exposure of 19 substances to lung A549 cells at the air liquid interface or under submerged conditions reveals high correlation between cytotoxicity in vitro and CLP classifications for acute lung toxicity. Toxicol. Lett. 316, 119–126. https://doi.org/10.1016/j.toxlet.2019.09.014.
Gornati, R., Colombo, G., Clerici, M., Rossi, F., Gagliano, N., Riva, C., Colombo, R., Dalle-Donne, I., Bernardini, G., Milzani, A., 2013. Protein carbonylation in human endothelial cells exposed to cigarette smoke extract. Toxicol. Lett. 218, 118–128. https://doi.org/10.1016/j.toxlet.2013.01.023.
Gregory, T.J., Longmore, W.J., Moxley, M.A., Whitsett, J.A., Reed, C.R., Fowler, A.A., Hudson, L.D., Maunder, R.J., Crim, C., Hyers, T.M., 1991. Surfactant chemical composition and biophysical activity in acute respiratory distress syndrome. J. Clin. Investig. 88, 1976–1981. https://doi.org/10.1172/JCI115523.
Günther, A., Siebert, C., Schmidt, R., Ziegler, S., Grimminger, F., Yabut, M., Temmesfeld, B., Walmrath, D., Morr, H., Seeger, W., 1996. Surfactant alterations in severe pneumonia, acute respiratory distress syndrome, and cardiogenic lung edema. Am. J. Respir. Crit. Care Med 153, 176–184. https://doi.org/10.1164/ajrccm.153.1.8542113.
Haider, S.R., Reid, H.J., Sharp, B.L., 2012. Tricine-SDS-PAGE. pp. 81–91. https://doi.org/10.1007/978-1-61779-821-4_8.
Haller, T., Ortmayr, J., Friedrich, F., Völkl, H., Dietl, P., 1998. Dynamics of surfactant release in alveolar type II cells. Proc. Natl. Acad. Sci. 95, 1579–1584. https://doi.org/10.1073/pnas.95.4.1579.
Hamaoui, D., Subtil, A., 2022. ATG16L1 functions in cell homeostasis beyond autophagy. FEBS J. 289, 1779–1800. https://doi.org/10.1111/febs.15833.
Hanrahan, J.W., Abu-Arish, A., Wong, F.H., Turner, M.J., Carlile, G.W., Thomas, D.Y., Cantin, A.M., 2022. Chronic obstructive pulmonary disease and the modulation of CFTR by acute exposure to cigarette smoke. Am. J. Physiol. Cell Physiol. 323, C1374–C1392. https://doi.org/10.1152/ajpcell.00356.2022.
Han, S., Mallampalli, R.K., 2015. The role of surfactant in lung disease and host defense against pulmonary infections. Ann. Am. Thorac. Soc. 12, 765–774. https://doi.org/10.1513/AnnalsATS.201411-507FR.
Hariri, M., Millane, G., Guimond, M.-P., Guay, G., Dennis, J.W., Nabi, I.R., 2000. Biogenesis of multilamellar bodies via autophagy. Mol. Biol. Cell 11, 255–268. https://doi.org/10.1091/mbc.11.1.255.
Higashi, T., Elmeligy, E., Mai, Y., Noya, Y., Terada, K., Mazaki, Y., Kuge, Y., Miwa, S., 2019. Glutathione and cysteines suppress cytotoxicity of gas phase of cigarette smoke by direct reacting with unsaturated carbonyl compounds in the gas phase. Biochem Biophys. Res Commun. 509, 988–993. https://doi.org/10.1016/j.bbrc.2019.01.040.
Higenbottam, T., 1989. Lung lipids and disease. Respiration 55, 14–27. https://doi.org/10.1159/000195747.
Hohlfeld, J., Fabel, H., Hamm, H., 1997. The role of pulmonary surfactant in obstructive airways disease. Eur. Respir. J. 10, 482–491. https://doi.org/10.1183/09031936.97.10020482.
Hohlfeld, J.M., 2001. The role of surfactant in asthma. Respir. Res 3, 4. https://doi.org/10.1186/rr176.
Hoshino, Y., Mio, T., Nagai, S., Miki, H., Ito, I., Izumi, T., 2001. Cytotoxic effects of cigarette smoke extract on an alveolar type II cell-derived cell line. Am. J. Physiol. Lung Cell. Mol. Physiol. 281, L509–L516. https://doi.org/10.1152/ajplung.2001.281.2.L509.
Hristova, V., Watson, A., Glover, M., Wang, J., Angermann, B., Ashenden, S., Bornot, A., Burke, H., Cellura, D., Chaerkady, R., Freeman, A., Mackay, A., Muthas, D., Novick, S., Öberg, L., Ostridge, K., Platt, A., Postle, A., Spalluto, C., Yu, W., Hess, S., Staples, K., Wilkinson, T., 2021. S90Comprehensive multiomics analysis demonstrates surfactant dysregulation in COPD. in: New Insights into Airways Disease. BMJ Publishing Group Ltd and British Thoracic Society, pp. A58.2–A59. https://doi.org/10.1136/thorax-2021-BTSabstracts.96.
Huang, Q., Li, Y., Li, C., Zhang, X., Du, X., Chen, Y., Corrigan, C.J., Wang, W., Ying, S., 2023. Cigarette smoke aggravates asthma via altering airways inflammation phenotypes and remodelling. Clin. Respir. J. 17, 1316–1327. https://doi.org/10.1111/crj.13718.
Huang, X., Liu, L., Yao, J., Lin, C., Xiang, T., Yang, A., 2024. *s* -acylation regulates *s*QSTM1/p62-mediated selective autophagy. Autophagy 20, 1467–1469. https://doi.org/10.1080/15548627.2023.2297623.
Hur, J., Rhee, C.K., Jo, Y.S., 2022. Effects of antioxidant on oxidative stress and autophagy in bronchial epithelial cells exposed to particulate matter and cigarette smoke extract. Tube Respir. Dis. (Seoul.) 85, 237–248. https://doi.org/10.4046/trd.2021.0152.
Im Hof, V., Gehr, P., Gerber, V., Lee, M.M., Schürch, S., 1997. In vivo determination of surface tension in the horse trachea and in vitro model studies. Respir. Physiol. 109, 81–93. https://doi.org/10.1016/S0034-5687(97)84032-7.
Jain, A., Mårtensson, J., Mehta, T., Krauss, A.N., Auld, P.A., Meister, A., 1992. Ascorbic acid prevents oxidative stress in glutathione-deficient mice: effects on lung type 2 cell lamellar bodies, lung surfactant, and skeletal muscle. Proc. Natl. Acad. Sci. 89, 5093–5097. https://doi.org/10.1073/pnas.89.11.5093.
Jiang, T., Harder, B., Rojo de la Vega, M., Wong, P.K., Chapman, E., Zhang, D.D., 2015. p62 links autophagy and Nrf2 signaling. Free Radic. Biol. Med 88, 199–204. https://doi.org/10.1016/j.freeradbiomed.2015.06.014.
Johansson, J., 1998. Structure and properties of surfactant protein c. Biochim. Et. Biophys. Acta (BBA) Mol. Basis Dis. 1408, 161–172. https://doi.org/10.1016/S0925-4439(98)00065-9.
Johansson, J., Curstedt, T., 1997. Molecular Structures and Interactions of Pulmonary Surfactant Components. Eur J Biochem 244, 675–693. https://doi.org/10.1111/j.1432-1033.1997.00675.x.
Kabore, A.F., Wang, W.-J., Russo, S.J., Beers, M.F., 2001. Biosynthesis of surfactant protein C: characterization of aggresome formation by EGFP chimeras containing propeptide mutants lacking conserved cysteine residues. J. Cell Sci. 114, 293–302. https://doi.org/10.1242/jcs.114.2.293.
Kageyama, S., Gudmundsson, S.R., Sou, Y.-S., Ichimura, Y., Tamura, N., Kazuno, S., Ueno, T., Miura, Y., Noshiro, D., Abe, M., Mizushima, T., Miura, N., Okuda, S., Motohashi, H., Lee, J.-A., Sakimura, K., Ohe, T., Noda, N.N., Waguri, S., Eskelinen, E.-L., Komatsu, M., 2021. p62/SQSTM1-droplet serves as a platform for autophagosome formation and anti-oxidative stress response. Nat. Commun. 12, 16. https://doi.org/10.1038/s41467-020-20185-1.
Kardorff, M., Mahler, H.-C., Huwyler, J., Sorret, L., 2023. Comparison of cell viability methods for human mesenchymal/stromal stem cells and human A549 lung carcinoma cells after freeze-thaw stress. J. Pharm. Toxicol. Methods 124, 107474. https://doi.org/10.1016/j.vascn.2023.107474.
Khanna, A.K., Xu, J., Mehra, M.R., 2012. Antioxidant N-acetyl cysteine reverses cigarette smoke-induced myocardial infarction by inhibiting inflammation and oxidative stress in a rat model. Lab. Investig. 92, 224–235. https://doi.org/10.1038/labinvest.2011.146.
Kim, H.J., Kang, S.U., Lee, Y.S., Jang, J.Y., Kang, H., Kim, C.-H., 2020. Protective effects of N-acetylcysteine against Radiation-Induced oral mucositis <I>In Vitro</I&gt. ltigt Vivolt/igt Cancer Res Treat. https://doi.org/10.4143/crt.2020.012.
Kim, Y.-H., An, Y.-J., Jo, S., Lee, S.-H., Lee, S.J., Choi, S.-J., Lee, K., 2018. Comparison of volatile organic compounds between cigarette smoke condensate (CSC) and extract (CSE) samples. Environ. Health Toxicol. 33, e2018012. https://doi.org/10.5620/eht.e2018012.
Kono, Y., Colley, T., To, M., Papaioannou, A.I., Mercado, N., Baker, J.R., To, Y., Abe, S., Haruki, K., Ito, K., Barnes, P.J., 2021. Cigarette smoke-induced impairment of autophagy in macrophages increases galectin-8 and inflammation. Sci. Rep. 11, 335. https://doi.org/10.1038/s41598-020-79848-0.
Korimilli, A., Gonzales, L.W., Guttentag, S.H., 2000. Intracellular localization of processing events in human surfactant protein b biosynthesis. J. Biol. Chem. 275, 8672–8679. https://doi.org/10.1074/jbc.275.12.8672.
Kosmider, B., Messier, E.M., Chu, H.W., Mason, R.J., 2011. Human alveolar epithelial cell injury induced by cigarette smoke. PLoS One 6, e26059. https://doi.org/10.1371/journal.pone.0026059.
Laganà, A.S., Unfer, V., Garzon, S., Bizzarri, M., 2020. Role of inositol to improve surfactant functions and reduce IL-6 levels: a potential adjuvant strategy for SARS-CoV-2 pneumonia? Med Hypotheses 144, 110262. https://doi.org/10.1016/j.mehy.2020.110262.
Lawson, W.E., Crossno, P.F., Polosukhin, V.V., Roldan, J., Cheng, D.-S., Lane, K.B., Blackwell, T.R., Xu, C., Markin, C., Ware, L.B., Miller, G.G., Loyd, J.E., Blackwell, T. S., 2008. Endoplasmic reticulum stress in alveolar epithelial cells is prominent in IPF: association with altered surfactant protein processing and herpesvirus infection. Am. J. Physiol. Lung Cell. Mol. Physiol. 294, L1119–L1126. https://doi.org/10.1152/ajplung.00382.2007.
Liao, C.-Y., Wu, T.-C., Yang, S.-F., Chang, J.T., 2021. Effects of NAC and gallic acid on the proliferation inhibition and induced death of lung cancer cells with different

antioxidant capacities. Molecules 27, 75. https://doi.org/10.3390/molecules27010075.
Liekkinen, J., Olżyńska, A., Cwiklik, L., Bernardino de la Serna, J., Vattulainen, I., Javanainen, M., 2023. Surfactant proteins SP-B and SP-C in pulmonary surfactant monolayers: physical properties controlled by specific Protein-Lipid interactions. Langmuir 39, 4338–4350. https://doi.org/10.1021/acs.langmuir.2c03349.
Lin, L., Lin, Y., Han, Z., Wang, K., Zhou, S., Wang, Z., Wang, S., Chen, H., 2024. Understanding the molecular regulatory mechanisms of autophagy in lung disease pathogenesis. Front Immunol. 15. https://doi.org/10.3389/fimmu.2024.1460023.
Lin, X., Wei, M., Song, F., Xue, D.I., Wang, Y., 2020. N-acetylcysteine (NAC) attenuating apoptosis and autophagy in RAW264.7 cells in response to incubation with mycolic acid from bovine mycobacterium tuberculosis complex. Pol. J. Microbiol 69, 223–229. https://doi.org/10.33073/pjm-2020-026.
Li, X., Wang, L., Hao, J., Zhu, Q., Guo, M., Wu, C., Li, S., Guo, Q., Ren, Q., Bai, N., Yi, F., Jiang, B., Zhang, W., Feng, Y., Xu, H., Jiang, H., Zhai, X., Zhang, G., Ji, H., Yang, X., Zhang, D., Fu, J., Chang, J., Song, X., Cao, L., 2022. The role of autophagy in lamellar body formation and surfactant production in type 2 alveolar epithelial cells. Int J. Biol. Sci. 18, 1107–1119. https://doi.org/10.7150/ijbs.64285.
Loret, T., Peyret, E., Dubreuil, M., Aguerre-Chariol, O., Bressot, C., le Bihan, O., Amodeo, T., Trouiller, B., Braun, A., Egles, C., Lacroix, G., 2016. Air-liquid interface exposure to aerosols of poorly soluble nanomaterials induces different biological activation levels compared to exposure to suspensions. Part Fibre Toxicol. 13, 58. https://doi.org/10.1186/s12989-016-0171-3.
Lystad, A.H., Carlsson, S.R., de la Ballina, L.R., Kauffman, K.J., Nag, S., Yoshimori, T., Melia, T.J., Simonsen, A., 2019. Distinct functions of ATG16L1 isoforms in membrane binding and LC3B lipidation in autophagy-related processes. Nat. Cell Biol. 21, 372–383. https://doi.org/10.1038/s41556-019-0274-9.
Mao, P., Wu, S., Li, J., Fu, W., He, W., Liu, X., Slutsky, A.S., Zhang, H., Li, Y., 2015. Human alveolar epithelial type II cells in primary culture. Physiol. Rep. 3, e12288. https://doi.org/10.14814/phy2.12288.
Markart, P., Ruppert, C., Wygrecka, M., Colaris, T., Dahal, B., Walmrath, D., Harbach, H., Wilhelm, J., Seeger, W., Schmidt, R., Guenther, A., 2007. Patients with ARDS show improvement but not normalisation of alveolar surface activity with surfactant treatment: putative role of neutral lipids. Thorax 62, 588–594. https://doi.org/10.1136/thx.2006.062398.
Mason, R.J., Voelker, D.R., 1998. Regulatory mechanisms of surfactant secretion. Biochim. Et. Biophys. Acta (BBA) Mol. Basis Dis. 1408, 226–240. https://doi.org/10.1016/S0925-4439(98)00070-2.
Mehlem, A., Hagberg, C.E., Muhl, L., Eriksson, U., Falkevall, A., 2013. Imaging of neutral lipids by oil red o for analyzing the metabolic status in health and disease. Nat. Protoc. 8, 1149–1154. https://doi.org/10.1038/nprot.2013.055.
Mehta, N.J., Marwah, P.K., Njus, D., 2019. Are proteinopathy and oxidative stress two sides of the same coin? Cells 8, 59. https://doi.org/10.3390/cells8010059.
Messier, E.M., Day, B.J., Kleeberger, S.R., Tuder, R.M., Bowler, R.P., Chu, H.W., Mason, R.J., Kosmider, B., 2013. *n* -Acetylcysteine protects murine alveolar type II cells from cigarette smoke injury in a *n*uclear erythroid 2–Related Factor–2–Independent manner. Am. J. Respir. Cell Mol. Biol. 48, 559–567. https://doi.org/10.1165/rcmb.2012-0295OC.
Mohan, J., Moparthi, S.B., Girard-Blanc, C., Campisi, D., Blanchard, S., Nugues, C., Rama, S., Salles, A., Pénard, E., Vassilopoulos, S., Wollert, T., 2024. ATG16L1 induces the formation of phagophore-like membrane cups. Nat. Struct. Mol. Biol. 31, 1448–1459. https://doi.org/10.1038/s41594-024-01300-y.
Morishita, H., Kanda, Y., Kaizuka, T., Chino, H., Nakao, K., Miki, Y., Taketomi, Y., Guan, J.-L., Murakami, M., Aiba, A., Mizushima, N., 2020. Autophagy Is Required for Maturation of Surfactant-Containing Lamellar Bodies in the Lung and Swim Bladder. Cell Rep 33, 108477. https://doi.org/10.1016/j.celrep.2020.108477.
Morishita, H., Kanda, Y., Mizushima, N., 2021. No air without autophagy: autophagy is important for lung and swim bladder inflation. Autophagy 17, 1040–1041. https://doi.org/10.1080/15548627.2021.1885148.
Nalayanda, D.D., Wang, Q., Fulton, W.B., Wang, T.H., Abdullah, F., 2010. Engineering an artificial alveolar-capillary membrane: a novel continuously perfused model within microchannels. J. Pedia Surg. 45, 45–51. https://doi.org/10.1016/J.JPEDSURG.2009.10.008.
Ning, B., Hang, S., Zhang, W., Mao, C., Li, D., 2023. An update on the bridging factors connecting autophagy and Nrf2 antioxidant pathway. Front Cell Dev. Biol. 11. https://doi.org/10.3389/fcell.2023.1232241.
NIST (Ed.), n.d. NIST/SEMATECH e-Handbook of Statistical Methods. ⟨http://www.itl.nist.gov/div898/handbook/⟩.
Nogee, L.M., Dunbar, A.E., Wert, S., Askin, F., Hamvas, A., Whitsett, J.A., 2002. Mutations in the surfactant protein c gene associated with interstitial lung disease. Chest 121, 20S–21S. https://doi.org/10.1378/chest.121.3_suppl.20S.
Nogee, L.M., Dunbar, A.E., Wert, S.E., Askin, F., Hamvas, A., Whitsett, J.A., 2001. A mutation in the surfactant protein c gene associated with familial interstitial lung disease. N. Engl. J. Med. 344, 573–579. https://doi.org/10.1056/NEJM200102223440805.
Öhlinger, K., Kolesnik, T., Meindl, C., Gallé, B., Absenger-Novak, M., Kolb-Lenz, D., Fröhlich, E., 2019. Air-liquid interface culture changes surface properties of A549 cells. Toxicol. Vitr. 60, 369–382. https://doi.org/10.1016/J.TIV.2019.06.014.
Olmeda, B., Martínez-Calle, M., Pérez-Gil, J., 2017. Pulmonary surfactant metabolism in the alveolar airspace: biogenesis, extracellular conversions, recycling. Ann. Anat. Anat. Anz. 209, 78–92. https://doi.org/10.1016/j.aanat.2016.09.008.
Ornatowski, W., Lu, Q., Yegambaram, M., Garcia, A.E., Zemskov, E.A., Maltepe, E., Fineman, J.R., Wang, T., Black, S.M., 2020. Complex interplay between autophagy and oxidative stress in the development of pulmonary disease. Redox Biol. 36, 101679. https://doi.org/10.1016/j.redox.2020.101679.
Osanai, K., Mizuno, S., Toga, H., Takahashi, K., 2020. Trafficking of newly synthesized surfactant protein b to the lamellar body in alveolar type II cells. Cell Tissue Res 381, 427–438. https://doi.org/10.1007/s00441-020-03232-7.
Patskan, G.J., Podraza, K.F., Meurrens, K., Coggins, C.R.E., Friedrichs, B., Gerstenberg, B., Gomm, W., Schnell, P., Stabbert, R., Veltel, D., Weber, S., Terpstra, P., 2008. Toxicological comparisons of three styles of a commercial U.S. Cigarette (Marlboro®) with the 1R4F reference cigarette. Inhal. Toxicol. 20, 695–721. https://doi.org/10.1080/08958370801935174.
Pérez-Gil, J., 2008. Structure of pulmonary surfactant membranes and films: The role of proteins and lipid–protein interactions. Biochimica et Biophysica Acta (BBA) - Biomembranes 1778, 1676–1695. https://doi.org/10.1016/j.bbamem.2008.05.003.
Petty, T.L., Ashbaugh, D.G., 1971. The adult respiratory distress syndrome. Chest 60, 233–239. https://doi.org/10.1378/chest.60.3.233.
Puthusseri, B., Marudamuthu, A., Tiwari, N., Fu, J., Idell, S., Shetty, S., 2017. Regulation of p53-mediated changes in the uPA-fibrinolytic system and in lung injury by loss of surfactant protein c expression in alveolar epithelial cells. Am. J. Physiol. Lung Cell. Mol. Physiol. 312, L783–L796. https://doi.org/10.1152/ajplung.00291.2016.
Racanelli, A.C., Kikkers, S.A., Choi, A.M.K., Cloonan, S.M., 2018. Autophagy and inflammation in chronic respiratory disease. Autophagy 14, 221–232. https://doi.org/10.1080/15548627.2017.1389823.
Rennard, S.I., 2004. Cigarette smoke in research. Am. J. Respir. Cell Mol. Biol. 31, 479–480. https://doi.org/10.1165/rcmb.F284.
Rodríguez-Pérez, J., Andreu-Martínez, R., Pérez-Sánchez, L., Hernández-García, A., Muñoz-Calleja, C., Cogolludo, Á., Calzada, M.J., 2025. CSE-Induced ER-Mitochondria crosstalk promotes oxidative stress and impairs bronchial contractile response. Antioxidants 14, 703. https://doi.org/10.3390/antiox14060703.
Ruifrok, A.C., Johnston, D.A., 2001. Quantification of histochemical staining by color deconvolution. Anal. Quant. Cytol. Histol. 23, 291–299.
Runwal, G., Stamatakou, E., Siddiqi, F.H., Puri, C., Zhu, Y., Rubinsztein, D.C., 2019. LC3-positive structures are prominent in autophagy-deficient cells. Sci. Rep. 9, 10147. https://doi.org/10.1038/s41598-019-46657-z.
Ryter, S.W., Choi, A.M.K., 2010. Autophagy in the lung. Proc. Am. Thorac. Soc. 7, 13–21. https://doi.org/10.1513/pats.200909-101JS.
Sano, H., Namekata, K., Kimura, A., Shitara, H., Guo, X., Harada, C., Mitamura, Y., Harada, T., 2019. Differential effects of N-acetylcysteine on retinal degeneration in two mouse models of normal tension glaucoma. Cell Death Dis. 10, 75. https://doi.org/10.1038/s41419-019-1365-z.
Savani, R.C., Godinez, R.I., Godinez, M.H., Wentz, E., Zaman, A., Cui, Z., Pooler, P.M., Guttentag, S.H., Beers, M.F., Gonzales, L.W., Ballard, P.L., 2001. Respiratory distress after intratracheal bleomycin: selective deficiency of surfactant proteins b and c. Am. J. Physiol. Lung Cell. Mol. Physiol. 281, L685–L696. https://doi.org/10.1152/ajplung.2001.281.3.L685.
Schmekel, B., Bos, J.A., Khan, A.R., Wohlfart, B., Lachmann, B., Wollmer, P., 1992. Integrity of the alveolar-capillary barrier and alveolar surfactant system in smokers. Thorax 47, 603–608. https://doi.org/10.1136/thx.47.8.603.
Schmitz, G., Müller, G., 1991. Structure and function of lamellar bodies, lipid-protein complexes involved in storage and secretion of cellular lipids. J. Lipid Res 32, 1539–1570.
Schürch, D., Ospina, O.L., Cruz, A., Pérez-Gil, J., 2010. Combined and independent action of proteins SP-B and SP-C in the surface behavior and mechanical stability of pulmonary surfactant films. Biophys. J. 99, 3290–3299. https://doi.org/10.1016/j.bpj.2010.09.039.
Schurch, S., Goerke, J., Clements, J.A., 1978. Direct determination of volume- and time-dependence of alveolar surface tension in excised lungs. Proc. Natl. Acad. Sci. USA 75, 3417–3421. https://doi.org/10.1073/PNAS.75.7.3417.
Scott, J.E., 2004. The pulmonary surfactant: impact of tobacco smoke and related compounds on surfactant and lung development. Tob. Induc. Dis. 2, 3. https://doi.org/10.1186/1617-9625-2-1-3.
Serrano, A.G., Pérez-Gil, J., 2006. Protein–lipid interactions and surface activity in the pulmonary surfactant system. Chem Phys Lipids 141, 105–118. https://doi.org/10.1016/j.chemphyslip.2006.02.017.
Shihan, M.H., Novo, S.G., Le Marchand, S.J., Wang, Y., Duncan, M.K., 2021. A simple method for quantitating confocal fluorescent images. Biochem Biophys. Rep. 25, 100916. https://doi.org/10.1016/j.bbrep.2021.100916.
Somborac-Bačura, A., van der Toorn, M., Franciosi, L., Slebos, D., Žanić-Grubišić, T., Bischoff, R., van Oosterhout, A.J.M., 2013. Cigarette smoke induces endoplasmic reticulum stress response and proteasomal dysfunction in human alveolar epithelial cells. Exp. Physiol. 98, 316–325. https://doi.org/10.1113/expphysiol.2012.067249.
Stachowicz-Kuśnierz, A., Korchowiec, B., Rogalska, E., Korchowiec, J., 2022. The lung surfactant activity probed with molecular dynamics simulations. Adv. Colloid Interface Sci. 304, 102659. https://doi.org/10.1016/j.cis.2022.102659.
Stahlman, M.T., Gray, M.P., Falconieri, M.W., Whitsett, J.A., Weaver, T.E., 2000. Lamellar body formation in normal and surfactant protein B-Deficient fetal mice. Lab. Investig. 80, 395–403. https://doi.org/10.1038/labinvest.3780044.
Stenger, P.C., Alonso, C., Zasadzinski, J.A., Waring, A.J., Jung, C.-L., Pinkerton, K.E., 2009. Environmental tobacco smoke effects on lung surfactant film organization. Biochim. Et. Biophys. Acta (BBA) Biomembr. 1788, 358–370. https://doi.org/10.1016/j.bbamem.2008.11.021.
Subramaniam, S., Whitsett, J.A., Hull, W., Gairola, C.G., 1996. Alteration of pulmonary surfactant proteins in rats chronically exposed to cigarette smoke. Toxicol. Appl. Pharm. 140, 274–280. https://doi.org/10.1006/taap.1996.0222.
Sukumaran, P., Nascimento Da Conceicao, V., Sun, Y., Ahamad, N., Saraiva, L.R., Selvaraj, S., Singh, B.B., 2021. Calcium signaling regulates autophagy and apoptosis. Cells 10, 2125. https://doi.org/10.3390/cells10082125.
Sun, X.W., Lin, Y.N., Ding, Y.J., Li, S.Q., Li, H.P., Zhou, J.P., Zhang, L., Shen, J.M., Li, Q. Y., 2022. Surfaxin attenuates PM2.5-induced airway inflammation via restoring

surfactant proteins in rats exposed to cigarette smoke. Environ. Res 203, 111864. https://doi.org/10.1016/j.envres.2021.111864.
Su, Y., Han, W., Giraldo, C., De Li, Y., Block, E.R., 1998. Effect of cigarette smoke extract on nitric oxide synthase in pulmonary artery endothelial cells. Am. J. Respir. Cell Mol. Biol. 19, 819–825. https://doi.org/10.1165/ajrcmb.19.5.3091.
Takano, M., Horiuchi, T., Nagai, J., Yumoto, R., 2012. Effect of cigarette smoke extract on insulin transport in alveolar epithelial cell line A549. Lung 190, 651–659. https://doi.org/10.1007/s00408-012-9413-9.
Tian, W., Alsaadi, R., Guo, Z., Kalinina, A., Carrier, M., Tremblay, M.-E., Lacoste, B., Lagace, D., Russell, R.C., 2020. An antibody for analysis of autophagy induction. Nat. Methods 17, 232–239. https://doi.org/10.1038/s41592-019-0661-y.
Tran, I., Ji, C., Ni, I., Min, T., Tang, D., Vij, N., 2015. Role of cigarette Smoke–Induced aggresome formation in chronic obstructive pulmonary Disease–Emphysema pathogenesis. Am. J. Respir. Cell Mol. Biol. 53, 159–173. https://doi.org/10.1165/rcmb.2014-0107OC.
Tyrrell, J., Ghosh, A., Manzo, N.D., Randell, S.H., Tarran, R., 2023. Evaluation of chronic cigarette smoke exposure in human bronchial epithelial cultures. J. Appl. Toxicol. 43, 862–873. https://doi.org/10.1002/jat.4430.
van Dam, L., Dansen, T.B., 2020. Cross-talk between redox signalling and protein aggregation. Biochem Soc. Trans. 48, 379–397. https://doi.org/10.1042/BST20190054.
van der Vaart, H., 2004. Acute effects of cigarette smoke on inflammation and oxidative stress: a review. Thorax 59, 713–721. https://doi.org/10.1136/thx.2003.012468.
Vij, N., Chandramani-Shivalingappa, P., Van Westphal, C., Hole, R., Bodas, M., 2018. Cigarette smoke-induced autophagy impairment accelerates lung aging, COPD-emphysema exacerbations and pathogenesis. Am. J. Physiol. Cell Physiol. 314, C73–C87. https://doi.org/10.1152/ajpcell.00110.2016.
Wang, H., Li, C., Peng, M., Wang, L., Zhao, D., Wu, T., Yi, D., Hou, Y., Wu, G., 2021. N-Acetylcysteine improves intestinal function and attenuates intestinal autophagy in piglets challenged with β-conglycinin. Sci. Rep. 11, 1261. https://doi.org/10.1038/s41598-021-80994-2.
Wang, L., van Iersel, L.E.J., Pelgrim, C.E., Lu, J., van Ark, I., Leusink-Muis, T., Gosker, H. R., Langen, R.C.J., Schols, A.M.W.J., Argilés, J.M., van Helvoort, A., Kraneveld, A.D., Garssen, J., Henricks, P.A.J., Folkerts, G., Braber, S., 2022. Effects of cigarette smoke on adipose and skeletal muscle tissue: in vivo and in vitro studies. Cells 11, 2893. https://doi.org/10.3390/cells11182893.
Wang, M., Zhang, Y., Xu, M., Zhang, H., Chen, Y., Chung, K.F., Adcock, I.M., Li, F., 2019. Roles of TRPA1 and TRPV1 in cigarette smoke -induced airway epithelial cell injury model. Free Radic. Biol. Med 134, 229–238. https://doi.org/10.1016/j.freeradbiomed.2019.01.004.
Wang, S., Wang, C., Yan, F., Wang, T., He, Y., Li, H., Xia, Z., Zhang, Z., 2017. N-Acetylcysteine attenuates diabetic myocardial ischemia reperfusion injury through inhibiting excessive autophagy. Mediat. Inflamm. 2017, 9257291. https://doi.org/10.1155/2017/9257291.
Wang, Y., Gao, X., Li, Yuan, Wang, X., Li, Yuanyuan, Zhang, S., Liu, H., Guo, H., Lu, W., Sun, D., 2021. Pulmonary surfactant-associated protein b regulates prostaglandin-endoperoxide synthase-2 and inflammation in chronic obstructive pulmonary disease. Exp. Physiol. 106, 1303–1311. https://doi.org/10.1113/EP089244.
Wasnick, R., Korfei, M., Piskulak, K., Henneke, I., Wilhelm, J., Mahavadi, P., Dartsch, R. C., von der Beck, D., Koch, M., Shalashova, I., Weiss, A., Klymenko, O., Askevold, I., Fink, L., Witt, H., Hackstein, H., El Agha, E., Bellusci, S., Klepetko, W., Königshoff, M., Eickelberg, O., Schermuly, R.T., Braun, T., Seeger, W., Ruppert, C., Guenther, A., 2023. Notch1 induces defective epithelial surfactant processing and pulmonary fibrosis. Am. J. Respir. Crit. Care Med 207, 283–299. https://doi.org/10.1164/rccm.202105-1284OC.
Weaver, T.E., 1998. Synthesis, processing and secretion of surfactant proteins B and C. Biochimica et Biophysica Acta (BBA) - Molecular Basis of Disease 1408, 173–179. https://doi.org/10.1016/S0925-4439(98)00066-0.
Weaver, T.E., Conkright, J.J., 2001. Function of Surfactant Proteins B and C. Annu Rev Physiol 63, 555–578. https://doi.org/10.1146/annurev.physiol.63.1.555.
Weaver, T.E., Na, C.-L., Stahlman, M., 2002. Biogenesis of lamellar bodies, lysosome-related organelles involved in storage and secretion of pulmonary surfactant. Semin Cell Dev. Biol. 13, 263–270. https://doi.org/10.1016/S1084952102000551.
Wert, S.E., Whitsett, J.A., Nogee, L.M., 2009. Genetic disorders of surfactant dysfunction. Pediatr. Dev. Pathol. 12, 253–274. https://doi.org/10.2350/09-01-0586.1.
Wong, K.K., Kua, K.P., Ooi, K.S., Cheah, F.C., 2023. The effects of N-acetylcysteine on lung alveolar epithelial cells infected with respiratory syncytial virus. Malays. J. Pathol. 45, 43–50.
YOO, M.O., JUNG, E.M., JEON, B.H., TRAN, D.N., JEUNG, E.B., 2020. Cigarette smoke extraxt influences intracellular calcium concentration in A549 cells. J. Physiol. Pharm. 71, 679–687.
Yu, S.H., Possmayer, F., 1996. Effect of pulmonary surfactant protein a and neutral lipid on accretion and organization of dipalmitoylphosphatidylcholine in surface films. J. Lipid Res 37, 1278–1288.
Zhang, L., Xu, J., Li, Y., Meng, F., Wang, W., 2024. Smoking on the risk of acute respiratory distress syndrome: a systematic review and meta-analysis. Crit. Care 28, 122. https://doi.org/10.1186/s13054-024-04902-6.
Zhang, S., Li, X., Xie, F., Liu, K., Liu, H., Xie, J., 2017. Evaluation of whole cigarette smoke induced oxidative stress in A549 and BEAS–2B cells. Environ. Toxicol. Pharm. 54, 40–47. https://doi.org/10.1016/j.etap.2017.06.023.
Zhang, S., Lu, X., Fang, X., Wang, Z., Cheng, S., Song, J., 2022. Cigarette smoke extract combined with LPS reduces ABCA3 expression in chronic pulmonary inflammation May be related to PPARγ/ P38 MAPK signaling pathway. Ecotoxicol. Environ. Saf. 244, 114086. https://doi.org/10.1016/j.ecoenv.2022.114086.
Zhang, Y., Huang, W., Zheng, Z., Wang, W., Yuan, Y., Hong, Q., Lin, J., Li, X., Meng, Y., 2021. Cigarette smoke-inactivated SIRT1 promotes autophagy-dependent senescence of alveolar epithelial type 2 cells to induce pulmonary fibrosis. Free Radic. Biol. Med 166, 116–127. https://doi.org/10.1016/j.freeradbiomed.2021.02.013.
Zhao, C., Fang, X., Wang, D., Tang, F., Wang, X., 2010. Involvement of type II pneumocytes in the pathogenesis of chronic obstructive pulmonary disease. Respir. Med 104, 1391–1395. https://doi.org/10.1016/j.rmed.2010.06.018.
Zhao, J., Han, M., Tian, Y., Zhao, P., Liu, X., Dong, H., Feng, S., Li, J., 2024. N-acetylcysteine attenuates cigarette Smoke-induced alveolar epithelial cell apoptosis through reactive oxygen species depletion and glutathione replenish in vivo and in vitro. Curr. Pharm. Biotechnol. 25, 1466–1477. https://doi.org/10.2174/0113892010257526231019143524.
Zhao, X., Zhang, Q., Zheng, R., 2022. The interplay between oxidative stress and autophagy in chronic obstructive pulmonary disease. Front Physiol. 13. https://doi.org/10.3389/fphys.2022.1004275.
Zhitkovich, A., 2019. *n* -Acetylcysteine: antioxidant, aldehyde scavenger, and more. Chem. Res Toxicol. 32, 1318–1319. https://doi.org/10.1021/acs.chemrestox.9b00152.
Zhong, Q., Zhou, B., Ann, D.K., Minoo, P., Liu, Y., Banfalvi, A., Krishnaveni, M.S., Dubourd, M., Demaio, L., Willis, B.C., Kim, K.-J., duBois, R.M., Crandall, E.D., Beers, M.F., Borok, Z., 2011. Role of endoplasmic reticulum stress in Epithelial–Mesenchymal transition of alveolar epithelial cells. Am. J. Respir. Cell Mol. Biol. 45, 498–509. https://doi.org/10.1165/rcmb.2010-0347OC.
Zong, D., Liu, X., Li, J., Ouyang, R., Chen, P., 2019. The role of cigarette smoke-induced epigenetic alterations in inflammation. Epigenetics Chromatin 12, 65. https://doi.org/10.1186/s13072-019-0311-8.